frontiers | Frontiers in Earth Science

TYPE Original Research
PUBLISHED 17 August 2022
DOI 10.3389/feart.2022.952690

OPEN ACCESS

EDITED BY
Omid Haeri-Ardakani,
Department of Natural Resources, Canada

REVIEWED BY
Mohammad Adnan Quasim,
Aligarh Muslim University, India
Ryan McAleer,
United States Geological Survey (USGS), United States

*CORRESPONDENCE
Abdulwahab Muhammad Bello,
abdulwahab.bello@kfupm.edu.sa

SPECIALTY SECTION
This article was submitted to Sedimentology, Stratigraphy and Diagenesis, a section of the journal Frontiers in Earth Science

RECEIVED 25 May 2022
ACCEPTED 20 July 2022
PUBLISHED 17 August 2022

CITATION
Bello AM, Charlaftis D, Jones SJ, Gluyas J, Acikalin S, Cartigny M and Al-Ramadan K (2022), Experimental diagenesis using present-day submarine turbidite sands.
Front. Earth Sci. 10:952690.
doi: 10.3389/feart.2022.952690

Experimental diagenesis using present-day submarine turbidite sands

Abdulwahab Muhammad Bello[1]*, Dimitrios Charlaftis[2], Stuart J. Jones[2], Jon Gluyas[2], Sanem Acikalin[3], Matthieu Cartigny[4] and Khalid Al-Ramadan[5]

[1]Center for Integrative Petroleum Research, College of Petroleum Engineering and Geoscience, King Fahd University of Petroleum and Minerals, Dhahran, Saudi Arabia, [2]Department of Earth Sciences, Durham University, Durham, United Kingdom, [3]School of Natural and Environmental Sciences, University of Newcastle, Newcastle Upon Tyne, United Kingdom, [4]Department of Geography, Durham University, Durham, United Kingdom, [5]Department of Geoscience, College of Petroleum Engineering and Geoscience, King Fahd University of Petroleum and Minerals, Dhahran, Saudi Arabia

Hydrothermal-reactor experiments were conducted to investigate the potential formation of chlorite and microquartz grain coatings on detrital quartz and feldspar grains, and to understand their role in inhibiting the formation of quartz and feldspar (albite) overgrowths. Modern-day proximal and distal unconsolidated sediment from the Bute Inlet (British Columbia, Canada) with known amounts of precursor clay content, were used as starting material. The samples were heated to 250°C at water vapour pressure in a hydrothermal reactor for 72 h. The experiments were performed with and without a silica supersaturated Na_2CO_3 (0.1 M) solution. Detailed microscopy and EDS mapping analysis identified that the main chlorite precursor, crucial for the formation of the synthesized grain coatings, was a Mg-rich chlorite. The experimental results showed that where the volume of precursor chlorite was low (i.e., 0.1%), notably in the proximal channel Bute samples, chlorite coatings were poorly developed, with a clay volume and maximum chlorite-coating coverage of 0.5% and 47%, respectively. In contrast, with an initial precursor chlorite volume of 14.5%, the distal lobe Bute sample has generated chlorite volume ranging from 42.9% to 56.3% post-experiment, with a maximum chlorite-coating coverage of 77%. The chlorite and microquartz coatings formed in the study are morphologically similar to those seen in natural sandstone reservoirs, and they have restricted the development of quartz and albite cementation in the reactor experiments. The findings provide quantitative data that can be utilised to describe diagenetic changes in mesodiagenetic environments.

KEYWORDS

Bute Inlet, diagenesis, chlorite coatings, microcrystalline quartz coatings, quartz overgrowths

Introduction

Authigenic quartz cement is one of the main porosity destroyers in deeply buried siliciclastic reservoirs (Houseknecht, 1987; McBride, 1989; Worden et al., 2000; Worden and Morad, 2000; Al-Ramadan et al., 2013a; Quasim et al., 2021). Grain-coating clays (e.g., chlorite, illite, and mixed-layer illite-smectite, etc.) and coatings of microcrystalline quartz have been identified as porosity-preserving cements (Pittman et al., 1992; Ehrenberg, 1993; Aase et al., 1996; Bloch et al., 2002; Saner et al., 2006; Taylor et al., 2010; French et al., 2012; Stricker and Jones, 2018). They inhibit the nucleation of quartz overgrowths by developing a diffusion barrier between the detrital quartz surface and the primary pore system, restricting silica supply to the detrital grain surface (Ajdukiewicz and Larese, 2012). The effectiveness of clay coatings in porosity preservation largely depends on their mineralogy, thickness, and extent (e.g., coverage) (Pittman et al., 1992; Lander and Walderhaug, 1999; Ajdukiewicz and Larese, 2012). Many studies on the role of clay coatings on reservoir quality preservation have primarily focused on the ability of the coatings to prevent the development of quartz cement on detrital quartz alone (Chen et al., 2011; Ajdukiewicz and Larese, 2012; Dutton et al., 2018). However, depending on sandstone compositions, albite overgrowths can develop on feldspar grains (Chowdhury and Noble, 1993; González-Acebrón et al., 2010; Khanam et al., 2021), growing into the pore space and reducing intergranular porosity, notably in arkosic sandstones. Consequently, understanding the formation of clay coatings on quartz and feldspar grains is important for comprehensive evaluation of reservoir quality in deeply buried sandstones.

Porosity-preserving clays in sandstones occur as detrital and authigenic coatings (Ehrenberg, 1993; Dutton et al., 2018; Stricker and Jones, 2018; Tang et al., 2018). Detrital clay coats develop in primary depositional environments, formed during or shortly after sediment deposition through, for instance, mechanical infiltration (Matlack et al., 1989; Al-Ramadan et al., 2013b; Al-Ramadan, 2014), or sediment dewatering in deep-water settings (Houseknecht and Pittman, 1992; Porten et al., 2019). Detrital clays in deep-water sandstones could also be inherited from continental, transitional, or shallow marine/shelf environments (Wilson, 1992; Bahlis and de Ros, 2013; Yezerski and Shumaker, 2018). Authigenic clay coats develop through direct precipitation (e.g., neoformation), thermally-driven recrystallization of precursor, detrital coats (Dutton et al., 2018), and through *in situ* development from alteration of detrital precursors (Aagaard et al., 2000; Ajdukiewicz and Larese, 2012; Haile et al., 2015). Smectite and berthierine, for instance, are widely reported as precursors for chlorite (Heald and Larese, 1974; Ahn et al., 1988; Aase et al., 1996; Aagaard et al., 2000; Worden and Morad, 2003; Haile et al., 2015; Worden et al., 2020; Charlaftis et al., 2021). Nonetheless, the role of precursor clay coatings and the amount required to form coatings that would significantly inhibit quartz cementation are poorly constrained in the literature.

Additionally, in ancient sandstones, the role played by detrital clay coatings in the formation of authigenic clay coatings cannot be accurately established due to their partial or complete transformation during burial diagenesis. For example, in the Palaeocene Forties Sandstone Member, Central North Sea, Bello et al. (2021) reported that it was challenging to determine the extent of transformation as well as the amount or volume of precursor detrital clay coats required to form complete authigenic coats that prevent the development of quartz overgrowths. This is because thermally-driven alteration of precursor, detrital smectite clay to form chlorite, illite, and mixed layer-illite smectite has occurred in the sandstones (Shaw and Conybeare, 2003; Bello et al., 2021). Thus, establishing the extent of coverage of detrital clay coats required to inhibit the development of quartz and feldspar cements is important for improving reservoir quality prediction (Bloch et al., 2002; Taylor et al., 2010).

Hydrothermal-reactor experiments on modern, deep-water sediment samples with known volume and coverage of precursor detrital clays can be a useful tool for understanding the transformation of precursor clays during diagenesis and improving reservoir quality prediction in ancient, deeply buried sandstones. Sediments from the modern-day, deep-water Bute Inlet, British Columbia, Canada were chosen because they are accessible and because they contain both submarine channel lobe deposits (Zeng et al., 1991; Hage, 2019; Heijnen et al., 2020), providing sediments with different volumes of precursor detrital clays. Following the experimental methodology developed by Charlaftis et al. (2021), and the modern-day Bute Inlet sediments, the present study aims to:

1) Test how detrital clay content affects the formation of grain-coating chlorite, by undertaking a series of hydrothermal-reactor experiments simulating burial diagenesis.
2) Establish the role of detrital clay and microcrystalline quartz coatings in arresting the formation of quartz overgrowths.
3) Provide quantitative data regarding the thickness and coverage of clay grain coatings, which can be used for diagenesis modelling to improve reservoir quality prediction.

Background geology of the Bute Inlet

The Bute Inlet, situated along the southwestern coast of British Columbia, Canada (Figures 1A,B), is about 80 km long and 4 km wide, ranging in water depths from 200 to 650 m. The Bute system has been recognized as a classic fjord, characterized by seafloor sedimentation that resembles those developed on large submarine fans (Zeng et al., 1991; Gales et al., 2018; Hage, 2019). The fjord is fed by Homathko and Southgate Rivers,

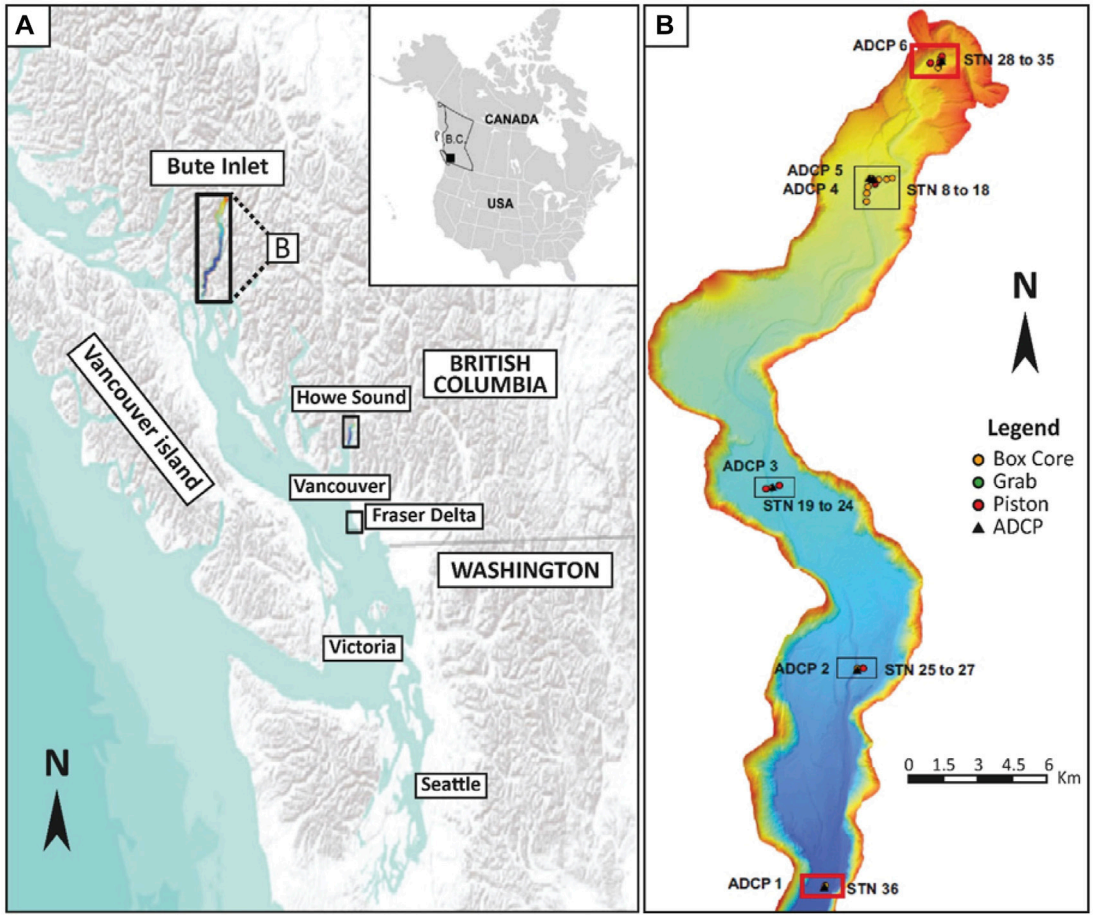

FIGURE 1
(A) Location of map of the Bute Inlet, British Columbia, Canada (modified after Esri USGS, NOAA). **(B)** Location of sampling points in the Bute Inlet. The samples used in this study were from Stations 028A and 036 (red boxes).

contributing 75% and 19% of the annual fresh water discharge into the fjord, respectively (Zeng et al., 1991). Turbidity currents in the Bute Inlet are initiated at the head of the fjord, on the fronts of the prograding and submerged delta of the Homathko and Southgate Rivers (Prior et al., 1987; Hage, 2019). The turbidity flows, linked to periods of high river discharge, may originate as slumps, moving downslope and transforming into turbidity currents, or as highly concentrated river flows. The downslope movement of the turbidity flows occurs through a single, sinuous, and long submarine channel (about 30 km long and 100–400 m wide) incised into the seafloor (Prior and Bornhold, 1989; Zeng et al., 1991).

Coarse-to fine-grained sands are largely remobilized from the delta fronts of the Homathko and Southgate Rivers and transported by turbidity currents up to 70 km from the head of the fjord (Prior and Bornhold, 1989; Zeng et al., 1991). Although it is relatively small and roughly linear, the modern Bute Inlet depositional system has been identified as an ideal site to study the link between rivers and deep-water sediment transport, with morphological features resembling those of many large, deep-sea fans (Zeng et al., 1991; Hage, 2019). The fjord is characterized by well-developed channel and lobe deposits. Additionally, it is relatively easy to access and sample, allowing for findings of experimental studies simulating deep-water flows, processes, and deposits to be tested and expanded in natural environments (Hughes Clarke, 2016).

Materials and methods

Sedimentary deposits

Sedimentary deposits of the Bute Inlet are categorized into four principal facies associations: spillover lobes, channel-lobe complex, distal splay, and basin floor, with facies typical of the

T_{a-e} divisions of the Bouma sequence (Bouma, 1962; Zeng et al., 1991). The samples used in the present study are from the channel-lobe complex facies associations alone, representing proximal channel Station 028A (STN 028A) and distal lobe Station 036 (STN 036) depositional environments (Figure 1B).

Sampling

Three syringe core sub-samples were collected from each of the proximal channel and distal lobe facies associations. The sample depth for STN 036 is 59 m and the depth for STN 028A is 330 m. The syringe sub-samples were further divided into three equal portions (e.g., 5 g). Two polished thin sections were made from the first portion of each facies for pre-experimental evaluation of the sediment framework composition, clay content, and possible cements. The remaining portions (2 for each sub-sample) were used for the hydrothermal reactor experiments. Post-experimental analysis was performed on polished thin sections of the reacted material. Although care was taken during the sediment core disaggregation and thin sections preparation, the two processes might have slightly disturbed the primary textural relationships of the loose sediments.

Analytical Procedures

The polished thin sections were carbon-coated, and SEM imaging was carried out using a Hitachi SU70 FEG scanning electron microscope (SEM), equipped with an Oxford Instruments energy dispersive X-ray spectrometer (EDS) at acceleration voltages of 12–15 kV and measured beam currents of 0.6–1.0 nA. Optical microscopy analysis was performed using a Leica DM2500P petrographic light microscope.

Six 2 × 2 mm EDS mineral maps at ×150 magnification (and 10% overlap) were acquired and analysed for both the pre- and post-experiment samples, enabling the quantitative and qualitative determination of the extent of the induced mineralogical transformations. The EDS mineral maps were acquired and processed using the Oxford Aztec software package. The maps were acquired at an acceleration voltage of 15 kV, pixel resolution of 1,024, process time of 3 s, pixel dwell time of 300 µs, and frame count of 1. Additionally, a binning factor of 2 was applied during the processing of the EDS mineral maps, which helped in identifying various mineral phases including, for instance, detrital and authigenic albites. The initial, processed EDS map for each experiment contained the area occupied by porosity, minerals, and unidentified mineral phases. Higher percentages of unidentified mineral phases were recorded in samples with more irregular sediment shape on the thin section slide, and vice versa. However, to have the true representation of the composition of the loose sediments, the modal analysis for each EDS map considered only the area occupied by the mineral phases, and excluded the area occupied by porosity and unidentified mineral phases.

Mineralogy of framework grains, microquartz, and clays was inferred from EDS analysis. In the cases of "clay coatings" an Fe-Mg rich aluminosilicate mineral with a platy morphology was identified and interpreted to be chlorite. Without XRD data, we cannot rule out that this could be another clay mineral (e.g., smectite or mixed-layer chlorite-smectite). However, for the purposes of this paper, the exact clay mineralogy does not affect our conclusions and, therefore, from here on, this is simply referred to as chlorite. EDS analysis for chlorite was conducted at an acceleration voltage of 20 kV, beam current of 0.6 nA, and process time of 4 s. Grain-coating chlorite composition was classified in terms of its Fe/(Fe+Mg) ratio (Hillier and Velde, 1992) based on elemental weight percentages of Fe and Mg determined using EDS analysis.

Chlorite- and microquartz-coatings coverage were measured on 50 randomly selected quartz and feldspar grains each using the Petrog (v. 4.5.9.2) and JMicrovision (v. 1.3.3) software packages based on the method described by Wooldridge et al. (2019) for modern-day sediments. ImageJ software was used to measure the thickness of clay and microquartz coatings, as well as grain size by measuring the long axis of 100 randomly selected quartz and feldspar grains. The grain size was determined using the SEM images of pre-experiment samples.

Hydrothermal experiments

The experiments were performed in a Parr Series 4560 Mini Reactor at the High-pressure High-temperature laboratory within the Integrated Chemical Reaction Facility (ICRF) at Durham University, following the experimental configuration described by Charlaftis et al. (2021). The modern-day Bute Inlet sediments were heated to 250°C in a 0.1 M Na_2CO_3 solution for 72 h at water vapour pressure (Table 1).

One sample from each station (i.e., 028A and 36; Table 1) was hydrothermally treated in a silica supersaturated solution resulted from the use of silica granules during the reaction. These granules also likely provided much of the silica for the nucleation of micro- and macro-quartz cements. The other samples from each station were treated without the silica granules (Table 1). The experiments were performed under strictly closed conditions, with subsequent cooling to room temperature after each run.

Results

Core description

The pre-reaction sediment sample from the proximal Station 028A (incised channel; Sample 1; Table 2) consists of dark to light

TABLE 1 Experimental conditions for the hydrothermal reactions.

Experiment	Core sample	Starting material	Solution (M)	Temperature (°C)	Duration (h)
1	Station 028A	Sediment + silica gel	0.1 Na_2CO_3	250	72
2	Station 028A	Sediment	0.1 Na_2CO_3	250	72
3	Station 036	Sediment + silica gel	0.1 Na_2CO_3	250	72
4	Station 036	Sediment	0.1 Na_2CO_3	250	72

The modern-day sediment samples are from the Bute Inlet, British Columbia, Canada.

TABLE 2 Results of the EDS mineral maps analyses showing sediments compositions before and after hydrothermal reactor experiments for the samples from Stations 028A and 036.

Sample	Sample 1 (pre-experiment) weight %	Sample 2 (experiment 1) weight %	Sample 3 (experiment 2) weight %	Sample 4 (pre-experiment) weight %	Sample 5 (experiment 3) weight %	Sample 6 (experiment 4) weight %	Min	Max	Av.
Sample location/ description	Station 028A (see Table 1 and Figure 1B)			Station 036 (see Table 1 and Figure 1B)					
Mineral/ parameter									
Quartz	31.0	30.4	28.5	19.3	15.8	10.4	10.4	31.0	22.6
K-feldspar	4.9	2.9	2.0	4.8	0.5	0.2	0.2	4.9	2.6
Plagioclase (Albite)	51.1	50.8	48.0	45.9	20.3	21.5	20.3	51.1	39.6
Mica	12.2	9.5	9.3	14.5	9.0	11.3	9.0	14.5	11.0
Pyrite	0.2	0.0	0.0	0.2	0.0	0.0	0.0	0.2	0.1
Rutile	0.5	0.2	1.1	0.0	0.0	0.0	0.0	1.1	0.3
Amphibole	0.0	0.0	0.0	0.5	0.2	0.2	0.0	0.5	0.2
Apatite	0.0	0.7	0.2	0.2	0.0	0.2	0.0	0.7	0.2
Authigenic Albite	0.0	1.1	8.4	0.0	0.0	0.0	0.0	8.4	1.6
Albite overgrowth	0.0	3.2	2.0	0.0	0.0	0.0	0.0	3.2	0.9
Quartz overgrowth	0.0	0.5	0.0	0.0	0.0	0.0	0.0	0.5	0.1
Microquartz	0.0	0.2	0.0	0.0	11.3	0.0	0.0	11.3	1.9
Chlorite	0.1	0.5	0.5	14.5	42.9	56.3	0.1	56.3	19.1
Average microquartz-coating coverage (%)					38				
Average chlorite-coating coverage (%)	Quartz = 18 Albite = 20	Quartz = 24 Albite = 15	Quartz = 47 Albite = 40	Quartz = 9 Albite = 17	Quartz = 46 Albite = 64	Quartz = 66 Albite = 77	Quartz= 9 Albite = 15	Quartz= 66 Albite = 77	
Chlorite average Fe/ (Fe+Mg) ratio	0.57			0.62					
Unidentified phases (%)	13.2	13.7	13.2	18.5	3.1	3.3	3.1	18.5	

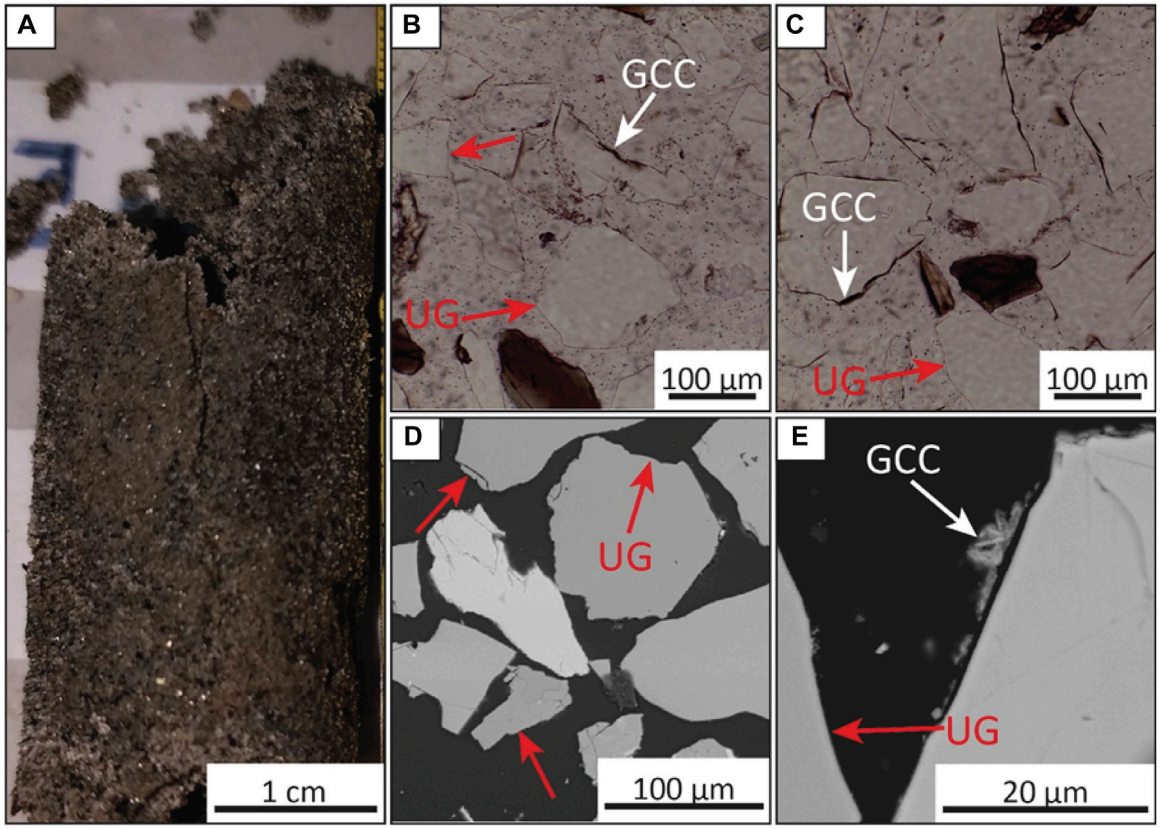

FIGURE 2
Images of samples from Station 028A. **(A)** Syringe core image of the proximal submarine channel from Station 028A. **(B,C)** Thin-section photomicrographs showing uncoated grains (UG; red arrows) and grain-coating chlorite (GCC; white arrows) in Sample 1. **(D)** BSE image showing uncoated detrital grains (Sample 1). **(E)** BSE image showing an uncoated grain (UG) and discontinuous, detrital grain-coating chlorite in Sample 1. (BSE, Backscattered Electron).

grey, massive, fine-to medium-grained sand (Figure 2A). Petrographic observations and SEM analysis reveal that the majority of the framework grains are not coated by chlorite (e.g., Figures 2B–E); however, a few grains have incomplete chlorite coatings (e.g., Figures 2C,E).

The initial sediment sample from Station 036 (distal lobe; Sample 4; Table 2) consists of grey, fine silt to very fine sand (Figure 3A). The detrital, framework grains of this sample are characterized by incomplete chlorite coatings (e.g., Figures 3B–E).

Mineralogical transformations

Table 2 summarizes the mineralogy of the pre- and post-reaction samples as quantified by EDS analysis (e.g., Figures 4A–F). The EDS mineral maps analysis of the pre-reaction Samples 1 and 4 reveal that the detrital framework grains consist of quartz (10.4%–31.0%), K-feldspar (0.2%–4.9%), plagioclase (20.3%–51.1%), and mica (9.0%–14.5%). Chlorite ranges from 0.1%to 56.3% and occurs as both grain-coating and pore-filling detrital matrix.

The volume of detrital quartz and plagioclase (albite) in the reacted and unreacted samples from Station 028A (Samples 1, 2, and 3; Table 2) have largely remained the same. Contrarily, quartz has decreased from 19.3% to 10.4% and albite from 45.9% to 20.3% in the samples from Station 036 (Samples 4, 5, and 6; Table 2).

The mineral maps analysis shows that K-feldspar content has decreased from 4.9% in Sample 1% to 2.9 % and 2.0% in Samples 2 and 3, respectively. The results show that the K-feldspar has transformed into albite (e.g., Figure 4F). Similarly, K-feldspar content has decreased from 4.8% in Sample 4 to 0.5 % and 0.2% in Samples 5 and 6, respectively. Additionally, diagenetic albite (1.1%–8.4%) occurs as overgrowths (Figures 4D, 5C) and as a replacement of K-feldspar (Figure 4F).

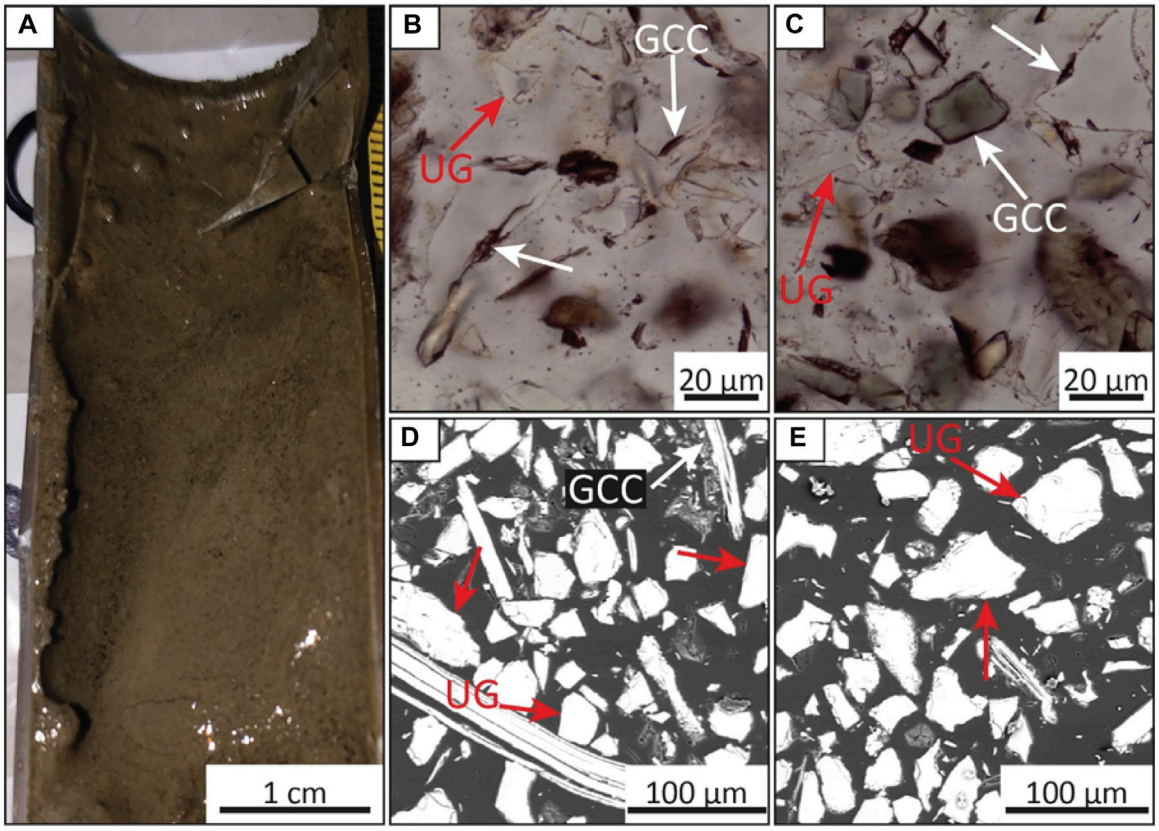

FIGURE 3
Images of samples from Station 036. **(A)** Syringe core image of the distal submarine lobe from Station 036. **(B,C)** Thin-section photomicrographs showing uncoated grains (UG; red arrows) and discontinuous grain-coating chlorite (GCC; white arrows) in Sample 4. **(D)** BSE image showing uncoated detrital grains and grain-coating chlorite (GCC) in Sample 4. **(E)** BSE image showing an uncoated grain (UG) and discontinuous, detrital grain-coating chlorite in Sample 4. (BSE, Backscattered Electron).

Chlorite occurs in trace amounts (e.g., 0.5%) in the reacted Samples 2 and 3 (Table 2; e.g., Figures 4C–F), forming discontinuous, incomplete coatings (e.g., Figures 5A–D). However, the volume of chlorite has significantly increased in the reacted Samples 5 and 6 (e.g., Figures 6C–F) to average volumes of 42.9 % and 56.3%, respectively from an initial value of 14.5% in the pre-reacted Sample 4 (Table 2; e.g., Figures 6A,B). As a result, chlorite coatings coverage is higher (46%–77%) in the post-reaction Samples 5 and 6 (Figures 6D, F, 7A, B, D; Table 2) than those in post-reaction Samples 2 and 3 (24%–47%) (Figures 4D,F; Table 2).

Although authigenic quartz overgrowths occur in trace amounts (0.5% average) in the silica-reacted Sample 2, it is absent in both post-reaction Samples 5 and 6. Microquartz (0.2%–11.3%) has precipitated in the silica-reacted Samples 2 and 5 as both pore-filling (e.g., Figures 5C, 7B) and grain-coating cement (e.g., Figure 7C).

Chlorite- and microquartz-coat coverage measurements

Results of the chlorite-coating coverage measurements for the pre- and post-reacted Samples 1 to 3 indicate that detrital quartz and albite grains have an average chlorite-coat coverage ranging from 18% to 47% and 20% to 40%, respectively (Table 2). Similarly, detrital quartz and albite grains in Samples 4 to 6 have average clay-coat coverage ranging from 9% to 66% and 17% to 77%, respectively (Table 2).

Furthermore, the results indicate that the reacted Samples 5 and 6 have higher clay-coating coverage than the reacted Samples 2 and 3 (Table 2). The mineral maps indicate that the pre-experiment Sample 1 has a total volume of precursor chlorite of 0.1%, whereas Sample 4 has a total volume of precursor chlorite of up to 14.5% (Table 2). In addition, the silica-reacted Samples 2 and 5 have less chlorite-coating coverage than those reacted without silica (Table 2).

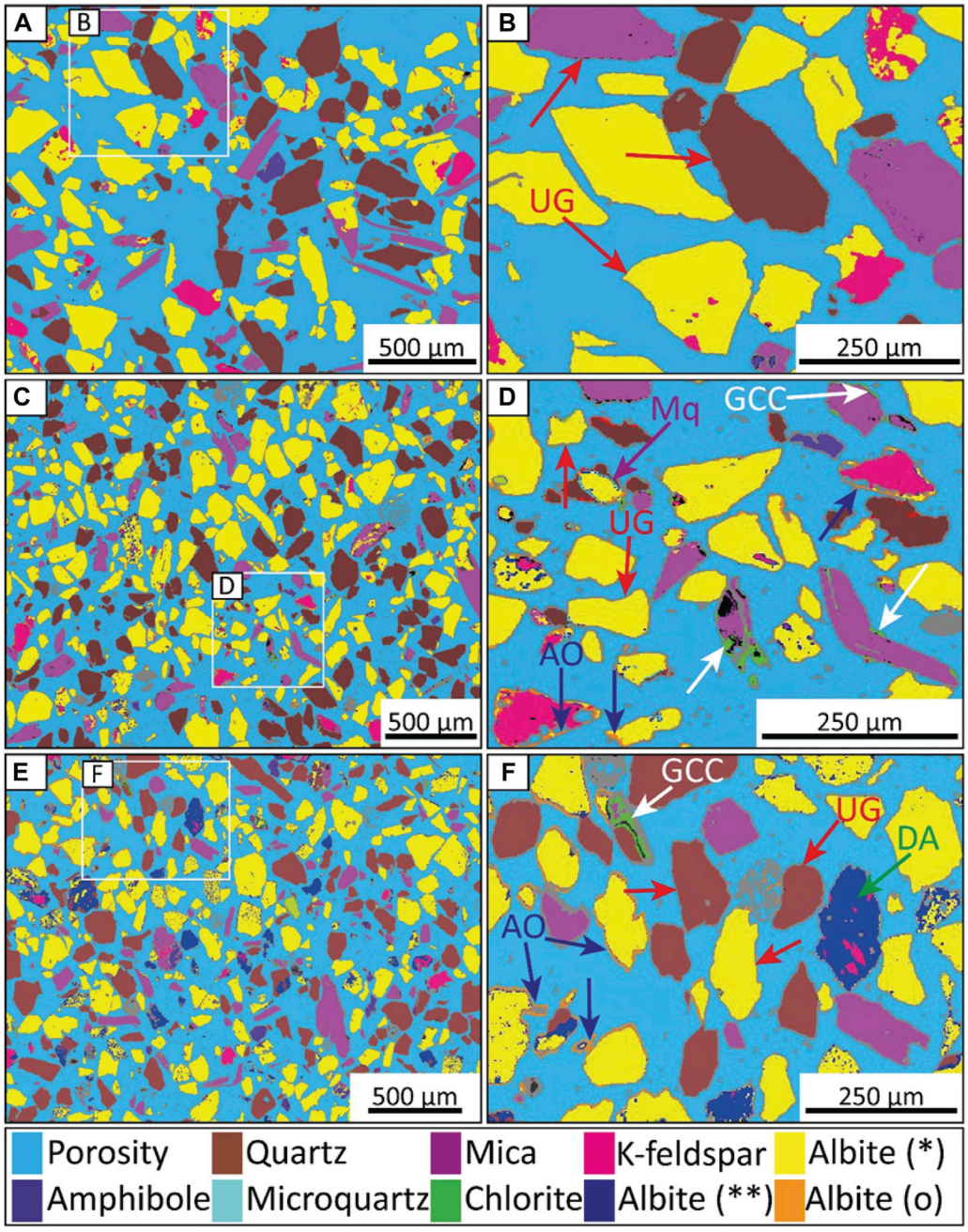

FIGURE 4
EDS mineral maps of the reacted and unreacted samples of Station 028A. **(A)** Processed EDS mineralogical map of the unreacted, pre-experiment Sample 1 showing the distribution of framework minerals. **(B)** Zoomed-in EDS mineral map of the inset in **(A)**. Note the uncoated grains (UG; red arrows) and the absence of grain-coating and pore-filling clays. **(C)** Analysed EDS mineral map of the post-experiment Sample 2. In this sample, chlorite coatings appear to be generally absent on the detrital grains. **(D)** Zoomed-in EDS mineral map of the inset in **(C)**. Notice the formation of albite overgrowths (AO) on K-feldspar grains, some coatings of microquartz (Mq) on grains, and the paucity of grain-coating chlorite (GCC) on detrital grains. **(E)** EDS mineral map of the post-experiment Sample 3. Grain-coating chlorite (GCC) appear to be generally absent on detrital grains. **(F)** Zoomed-in EDS mineral map of the inset in **(E)**. Note the development of diagenetic albite (DA) on partially to pervasively dissolved detrital plagioclase (albite) and K-feldspar grains. (*, Detrital albite; **, Diagenetic albite; o, Albite overgrowth).

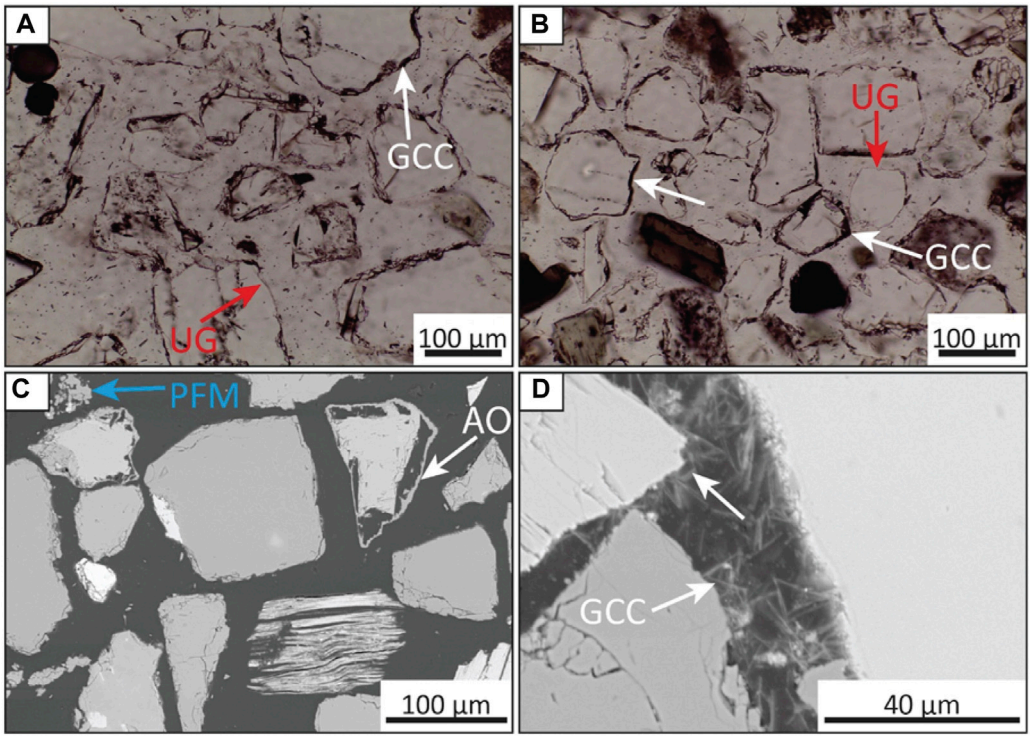

FIGURE 5
Thin-section photomicrographs and BSE images of the reacted samples from Station 028A. **(A,B)** Photomicrographs of the reacted Sample 3 showing uncoated grains (UG) and generally discontinuous grain-coating chlorite (GCC). **(C)** BSE image showing an albite overgrowth (AO) and pore-filling microcrystalline (PFM) in the silica-reacted Sample 2. **(D)** BSE image showing grain-coating chlorite (GCC) growing perpendicular to grain surfaces, into the pore and occluding intergranular porosity in the reacted Sample 3. (BSE, Backscattered Electron).

Measurement of microquartz-coating coverage indicates that Sample 5 has an average coating coverage of 38% (Table 2).

Detrital and experimental clays

Based on SEM morphological characteristics and EDS mineral maps analysis, chlorite is the detrital and authigenic clay mineral (Figures 8A–F). However, while precursor detrital clay coatings, experimental chlorite coats, and pore-filling chlorite in the pre- and post-experiment Samples 4 to 6 are more abundant and well-developed, those in Samples 1 to 3 occur in trace amounts (<1%) (Table 2). The chlorite occurs as grain-coating (Figures 8A,B, 9A–D–D), pore-filling (Figure 8C), and as replacement of detrital feldspar (Figure 8D), mica (biotite; Figure 8E), and clay matrix (Figure 8F). Authigenic, grain-coating chlorite grows in two forms: parallel (Figures 8A, 9A–D–D) and perpendicular to grain surface (e.g., Figures 5D, 8B, 9C). 1) Grain-coating chlorite parallel to grain surface. The coatings show a significant increase in clay-coating coverage (Figures 6D,F; Table 2), notably in the reacted Sample 6. 2) Authigenic grain-coating chlorite growing perpendicular to detrital quartz and feldspars (e.g., Figures 8B, 9C). Additionally, chlorite has been observed to replace or grow from pore-filling clay matrix (Figure 8F). Some grain-replacive chlorite, which replace feldspar and mica grains, exhibit a fan-like morphology (e.g., Figures 8D,E).

Under an optical microscope, grain-coating chlorite appears as dark brown coats around detrital grains in both plane and cross-polarized lights (Figures 9A,B) and grows either parallel (Figures 9A,B) or perpendicular (Figure 9C) to grain surfaces. The perpendicular chlorite often exhibits fan-like morphology (Figure 9C). The coats might be continuous (Figures 8A, 9C) or discontinuous (Figure 8B), with some grains being completely uncoated (Figure 9D).

The thickness of chlorite coats ranges from 2 to 13 µm (average 6 µm) and 0.7 to 27 µm (average 7 µm) in Samples 2 and 3, respectively. Similarly, in Samples 5 and 6, chlorite thickness ranges from 2 to 7 µm (average 5 µm) and 1 to 7 µm (average 3 µm), respectively.

The results of the measurements of Fe/(Fe + Mg) ratio conducted on precursor chlorite coats of pre-reacted Samples 1 and 4 show that the chlorite coatings are Mg-rich (Hillier and Velde, 1992; Grigsby, 2001) (Figures 10A–D), with an average Fe/(Fe + Mg) ratio of 0.57 (Figure 10B) and 0.62 (Figure 10D), respectively.

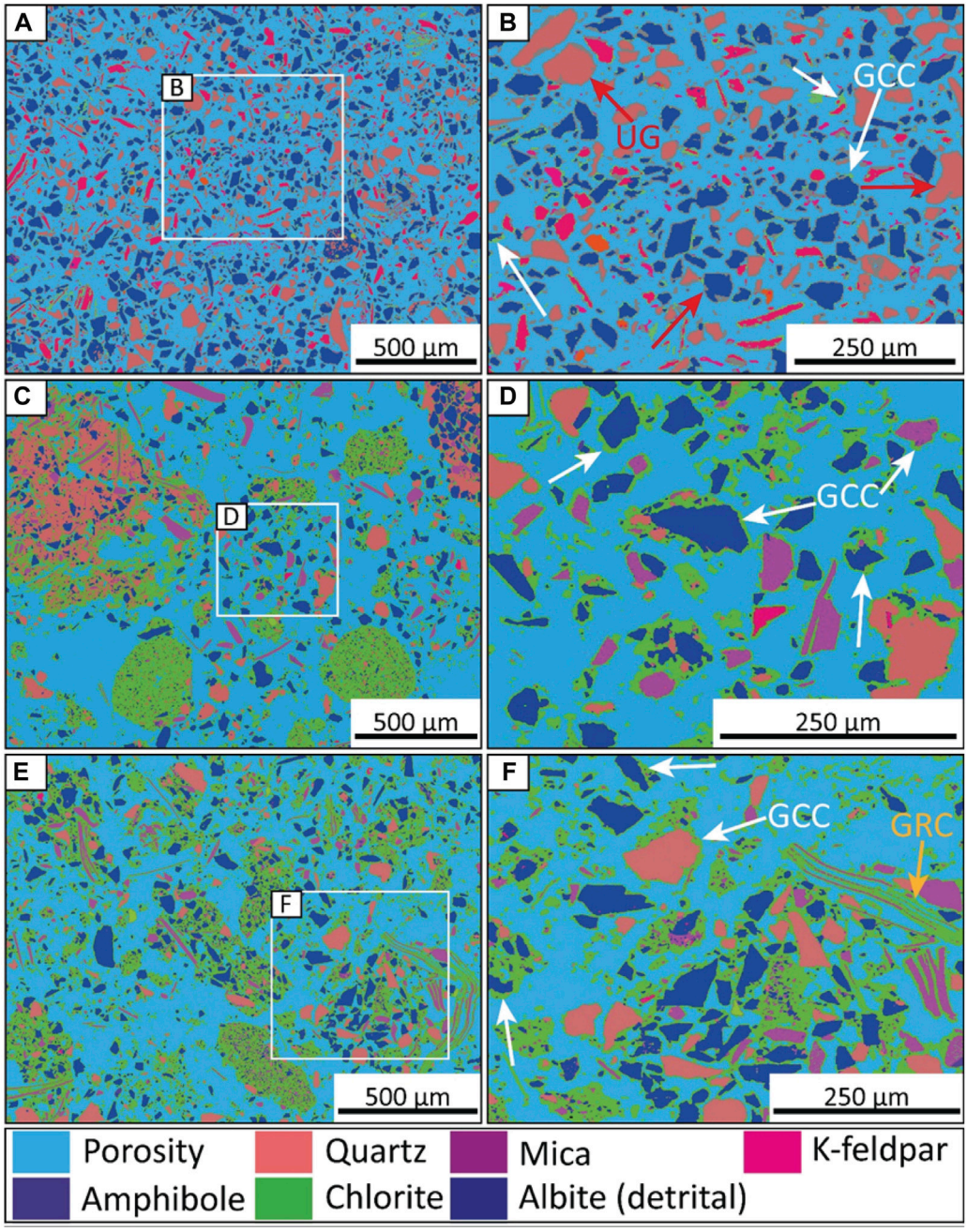

FIGURE 6
EDS mineral maps of the reacted and unreacted samples of Station 036. **(A)** Processed EDS mineralogical map of the unreacted, pre-experiment Sample 4 showing the distribution of framework minerals. **(B)** Zoomed-in EDS mineral map of the inset in **(A)**. Note the uncoated grains (UG; red arrows) and the general lack of grain-coating chlorite (GCC). **(C)** Analysed EDS mineral map of the reacted Sample 5 showing the distribution of framework and diagenetic minerals. **(D)** Zoomed-in EDS mineral map of the inset in **(C)**. Notice the well-developed grain-coating chlorite (GCC) on detrital grains. **(E)** EDS mineral map of the post-experiment Sample 6 showing the distribution of framework and diagenetic minerals. **(F)** Zoomed-in EDS mineral map of the inset in **(E)**. In this image, grain-coating chlorite (GCC) appear to be well-developed on detrital grains, and note the grain-replacive chlorite (GRC) replacing mica.

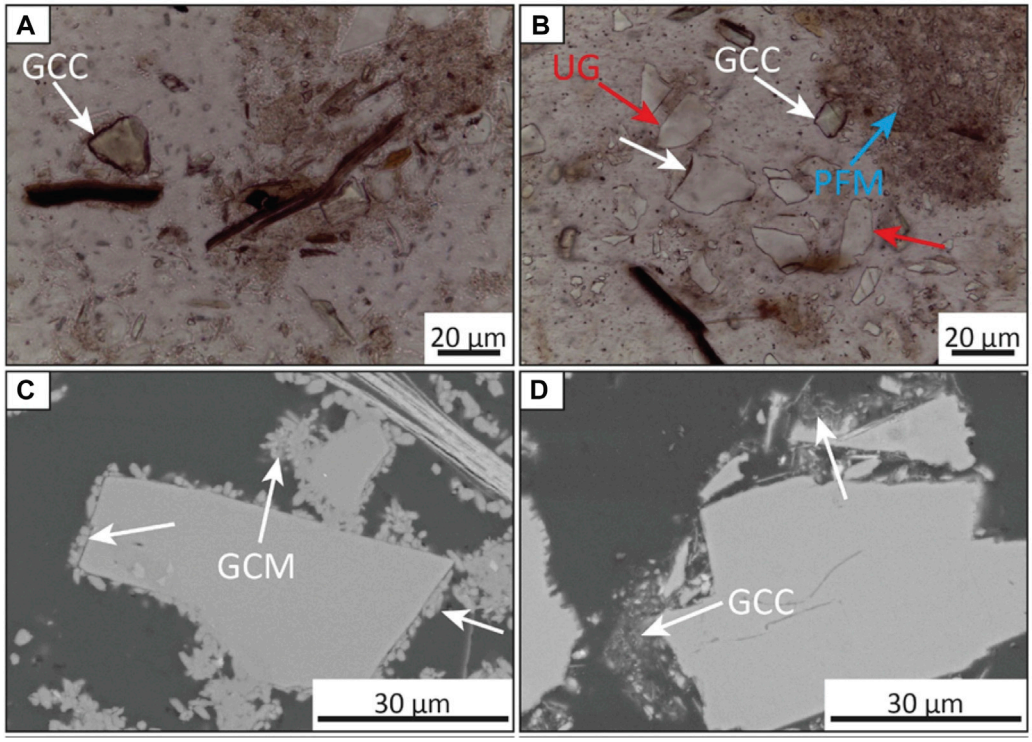

FIGURE 7
Thin-section photomicrographs and BSE images of the reacted samples from Station 036. **(A,B)** Photomicrographs of the reacted Sample 5 showing grain-coating chlorite (GCC), uncoated grains (UG), and pore-filling microcrystalline quartz (PFM). **(C)** BSE image showing well-developed, grain-coating microcrystalline quartz (GCM) in the silica-reacted Sample 5. **(D)** BSE image showing grain-coating chlorite (GCC) preventing quartz cementation in the reacted Sample 6. (BSE, Backscattered Electron).

Albite cement

Authigenic albite occurs as replacement of partly or pervasively dissolved detrital plagioclase and K-feldspar (e.g., Figures 11A,B), and as overgrowths on feldspars (Figures 5C, 11C,D). Albite precipitates as thin (Figure 11C) or thick (Figure 11D) overgrowths on detrital plagioclase or K-feldspars, with thicknesses of the overgrowths ranging from 0.4 to 32 µm (average 7.8 µm). The overgrowths, which may or may not be compositionally identical to their host detrital grains, often grow into partly or pervasively dissolved, host feldspar grains, (e.g., Figure 11C). In addition, the overgrowths are often identified based on BSE brightness, where they appear darker than their host grains (e.g., K-feldspar) (Figures 11C,D) Occasionally, the overgrowths surrounding moldic pore (MP) were developed from the post-overgrowth dissolution of detrital K-feldspar or plagioclase host grains (Figures 11E,F). On the other hand, grain-replacive albite replaces both dissolved plagioclase and K-feldspar grains. The replacement occurs as blocky, irregular albite on plagioclase or K-feldspar grains (e.g., Figure 11A), as pervasive replacement of dissolved K-feldspar (e.g., Figure 11B), or as thin, vein-like albite on K-feldspar grains.

Quartz overgrowths and microcrystalline quartz cement

Angular, blocky authigenic quartz overgrowths were observed only in the proximal-channel, silica-reacted Sample 2 (Figures 12A,B). The authigenic quartz overgrowths were developed where clays and microcrystalline quartz coatings are absent on detrital quartz grains (e.g., Figures 12A,B).

The influence of silica in the silica-reacted sediments of the Bute Inlet has led to the development of two main habits: 1) micro-quartz coatings (Figure 12C); and 2) intergranular pore-filling microcrystalline (Figure 12D). The lengths of microquartz crystals range from 1 to 6 µm (average 3 µm) and 1–7 µm (average 3 µm) for Sample 2 and Sample 5, respectively. The microquartz coatings cover detrital grains, such as biotite (Figure 12C), albite (Figure 12E), and quartz (Figure 12F). EDS mineral map data from Experiment 1 (Sample 2) shows that the total microquartz content is 0.2% (Table 2). However, in Experiment 3 (Sample 5), the volume of microquartz is higher (e.g., 11.3%). The intergranular pore-filling microcrystalline consists of randomly oriented crystal aggregates similar in size and habit to the grain-coating microquartz (Figure 12D).

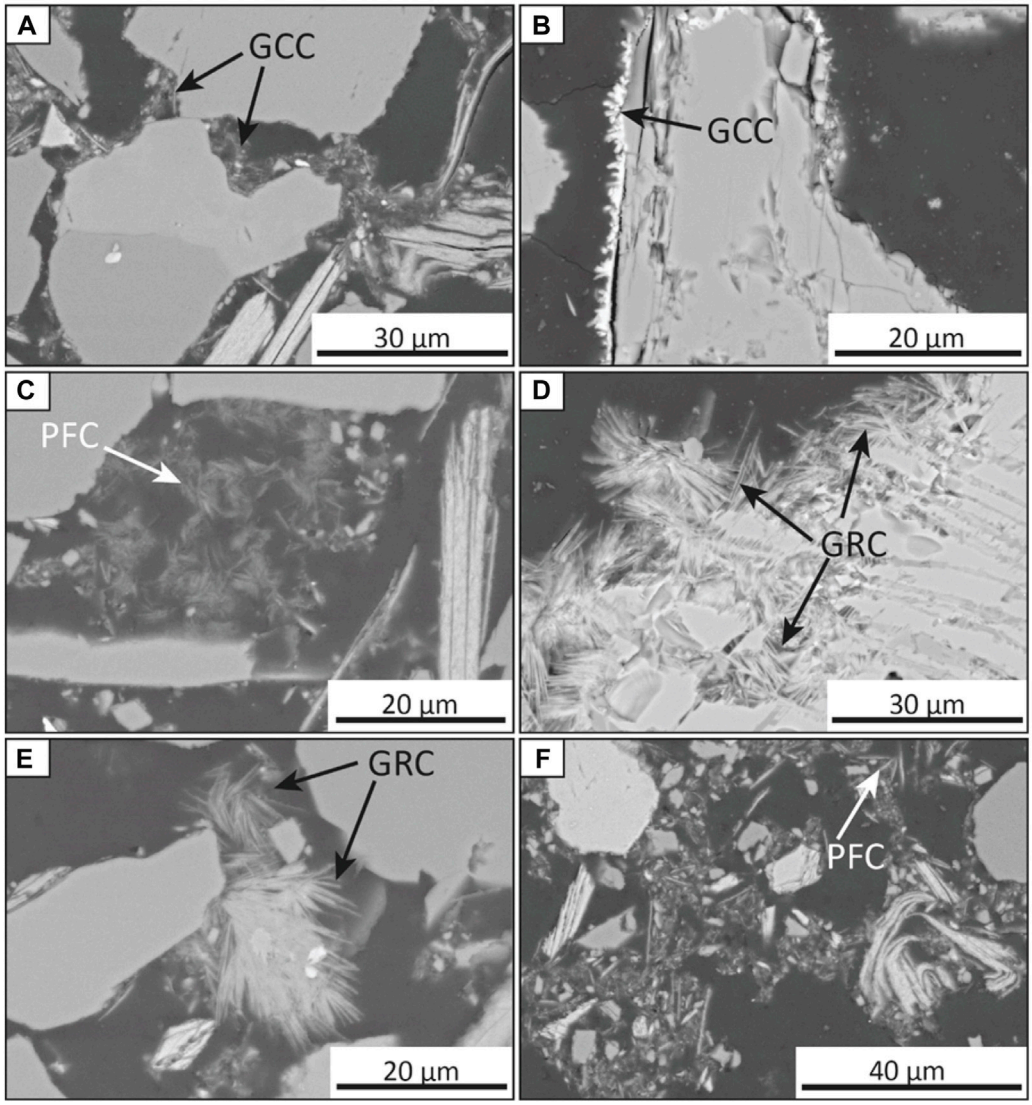

FIGURE 8
BSE images showing examples of grain-coating, pore-filling, and grain-replacing chlorite in the reacted samples of the Bute Inlet. **(A)** BSE image of authigenic grain-coating chlorite (GCC), growing parallel to quartz grain surface and from a precursor chlorite coat, (Sample 6). **(B)** BSE image of neoformed grain-coating chlorite (GCC) growing perpendicular to a detrital albite grain surface (Sample 6). **(C)** BSE image showing pore-filling chlorite (PFC) destroying intergranular porosity (Sample 5). **(D)** BSE image of grain-replacive chlorite (GRC), replacing partly dissolved K-feldspar (Sample 3). **(E)** BSE image showing a fan-like, grain-replacive chlorite (GRC), replacing detrital biotite (Sample 5). **(F)** BSE image showing pore-filling chlorite (PFC) growing from or replacing precursor pore-filling chlorite, probably Mg-rich chlorite (Sample 6). (BSE, Backscattered Electron).

Discussion

Impact of albitization of feldspars on reservoir quality

Albitization of detrital feldspar is an important diagenetic process in deeply-buried, arkosic sandstones (Saigal et al., 1988; Morad et al., 1990, 2000; Chowdhury and Noble, 1993; González-Acebrón et al., 2010). Our experiments have shown that blocky, thick albite overgrowths develop on detrital feldspars uncoated by chlorite and microcrystalline quartz coatings, growing into pore space (e.g., Figure 11D). The blocky, irregular albitization textures are similar to those described by (Chowdhury and Noble, 1993) from Early Carboniferous sandstones of the Abert Formation, Moncton sub-basin, South-eastern New Brunswick; and those described by (Milliken et al., 1989) from the Texas Gulf Coast sandstones, with the volumes of albite cement ranging from 2% to 3% and 3% to 4%, respectively.

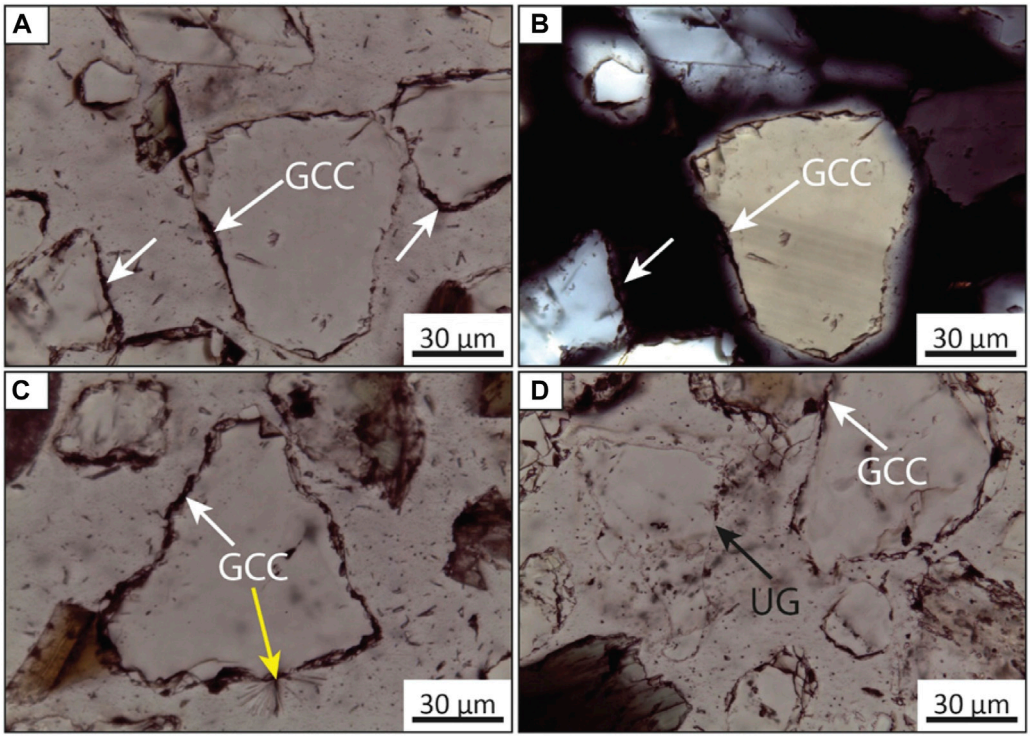

FIGURE 9
High-resolution, thin-section photomicrographs of grain-coating chlorite. **(A)** Plane polarized light (PPL) image of grain-coating chlorite (GCC) on detrital grains showing largely continuous coat. **(B)** Cross-polarized light (XPL) image of **(A)**. **(C)** Well-developed grain-coating chlorite (GCC) on detrital quartz, growing both parallel (white arrow) and perpendicular to grain surface (yellow arrow). **(D)** Plane polarized light (PPL) image showing coated and uncoated detrital grains (UG). Note that these images were from the reacted Sample 3.

Furthermore, whereas albite overgrowths reduce primary intergranular porosity, K-feldspar and plagioclase dissolution increases secondary porosity. Nevertheless, feldspar dissolution can significantly affect the original framework composition of sandstones, resulting in the formation of several diagenetic cements such as kaolinite, illite, dickite, and calcite (Boles, 1982; Saigal et al., 1988; Morad et al., 1990; Al-Ramadan, 2021). The decrease in feldspar content, particularly in the reacted Sample 5 and 6 (Table 2), the silica-rich solution in Sample 5, and the corresponding increase in the amount of grain-coating and pore-filling chlorite, suggests that feldspar dissolution and the silica-rich solution have supplied the silica required for the formation of the experimental chlorite. The albitization of feldspars replaces and occludes the secondary, dissolution porosity by growing into the pores (e.g. Figures 11C,D), thereby reducing reservoir quality (Chowdhury and Noble, 1993). Therefore, understanding the processes of dissolution and albitization of feldspars in sandstones is useful for the effective evaluation of reservoir quality and establishing the mass transport of Na^+ in the subsurface (Chowdhury and Noble, 1993).

Experimental development of clay and microquartz coatings

Authigenic chlorite coatings were hydrothermally synthesized on detrital quartz and feldspar grains (e.g., Figures 8B, 9C), and where coatings are absent, quartz and albite overgrowths were formed, respectively (e.g., Figures 11C, D, 12A, B). The experiments have shown that the physical obstruction of nucleation sites by the clay coats is an effective mechanism by which the development of ubiquitous quartz and albite overgrowths can be inhibited (Aagaard et al., 2000; Ajdukiewicz and Larese, 2012; Haile et al., 2015; Charlaftis et al., 2021; Charlaftis et al., 2022).

Two possible precursors for chlorite have been identified: 1) grain-coating and pore-filling Mg-rich chlorite (Figures 10A–D) and 2) dissolved or altered detrital mica (biotite) (Figure 8E). Results of the Fe/(Fe+Mg) ratio (Table 2) for chlorites have shown that the chlorites are both Mg- and Fe-rich, indicating that they were probably sourced from smectite (due to substantial amounts of Na, K, and Ca) and other Fe-rich grains (e.g., biotite and amphibole), respectively. Furthermore, the results of the hydrothermal reactor experiments (e.g., Experiment 4; Tables 1,

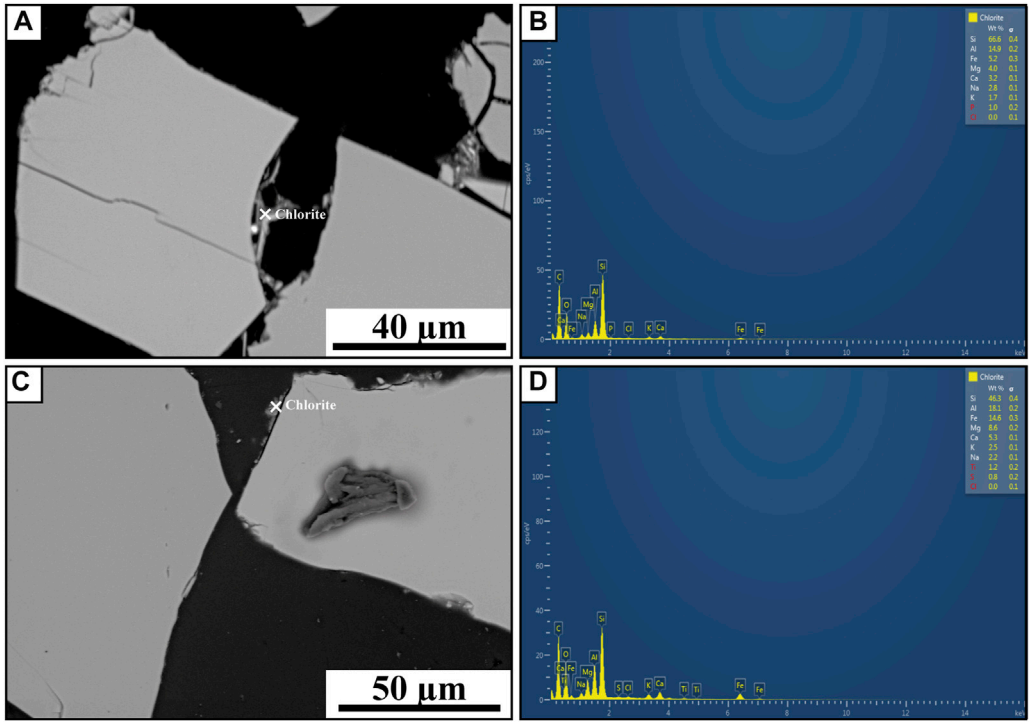

FIGURE 10
SEM images and EDS spectra for precursor, mg-rich chlorite coats. **(A)** SEM image showing precursor chlorite coating detrital grain (Sample 1). **(B)** EDS spectra for the Mg-rich chlorite coat in **(A)**. **(C)** SEM image showing precursor, Mg-rich chlorite coating detrital grain (Sample 4). **(D)** EDS spectra for the Mg-rich chlorite coat in **(C)**.

2) in Samples 5 and 6 (Table 2) suggest that the precursor chlorite was crucial for the formation of well-developed, diagenetic chlorite. However, because such precursor chlorite was insufficient in Samples 2 and 3 (Experiments 1 and 2, respectively), minor chlorite (<1%) was formed (Table 2; Figures 4D,F), resulting in low chlorite-coat coverage. This further suggests that the precursor chlorite, occurring as both coatings and pore-filling matrix in the first place, was more crucial in the formation of chlorite than biotite, despite the sufficient amount of biotite in the pre- and post-reacted Samples 1 to 3 (Table 2).

Chlorite coatings that were better-developed on detrital quartz and feldspars occur near altered mica grains (e.g., Figures 6F, 8C, E), suggesting that the altered mica grains (biotite) have acted as precursor for chlorite (Worden et al., 2020; Bello et al., 2022). While grain-coating chlorite appears to have prevented quartz and albite cementation, pore-filling chlorite, resulting from alteration of mica and detrital clay matrix, seem to have significantly occluded intergranular porosity (Figures 8C, F).

In Experiment 3 (Tables 1, 2), microquartz coatings precipitated and have prevented the development of quartz overgrowths (e.g., Figure 12F) (Aase et al., 1996; Jahren and Ramm, 2000; Weibel et al., 2010; French et al., 2012; French and Worden, 2013; French et al., 2021). Additionally, the microquartz coatings have precipitated on detrital feldspar grains, inhibiting the development of authigenic feldspar (albite) overgrowth (Figure 12E). Pore-filling microcrystalline, nonetheless, have occluded intergranular porosity (Figure 12D).

In ancient sandstones, microquartz coatings were interpreted to have formed in sands rich in biogenic silica (e.g., sponge spicules) (Hendry and Trewin, 1995; Aase and Walderhaug, 2005) during shallow burial diagenesis at a temperature of 50°C (Vagle et al., 1994). In the present study, microquartz coatings have been observed to be engulfed by chlorite coats (Figure 6C), indicating that they predate chlorite coatings, which form at ~100°C (Charlaftis et al., 2021). Furthermore, grain-coating microcrystalline quartz have been identified as an effective mechanism for porosity preservation in deeply buried sandstone reservoirs (Aase et al., 1996; Weibel et al., 2010; French et al., 2012; French and Worden, 2013); they help in stabilizing grain-grain contacts, thereby increasing sandstones resistance to pressure dissolution and preserving intergranular porosity (Lima and De Ros, 2002). The optimum coatings thickness ranges between 5 and 10 µm and the optimum volume between 4% and 6% (Lima and De Ros, 2002), similar to the findings of the present study.

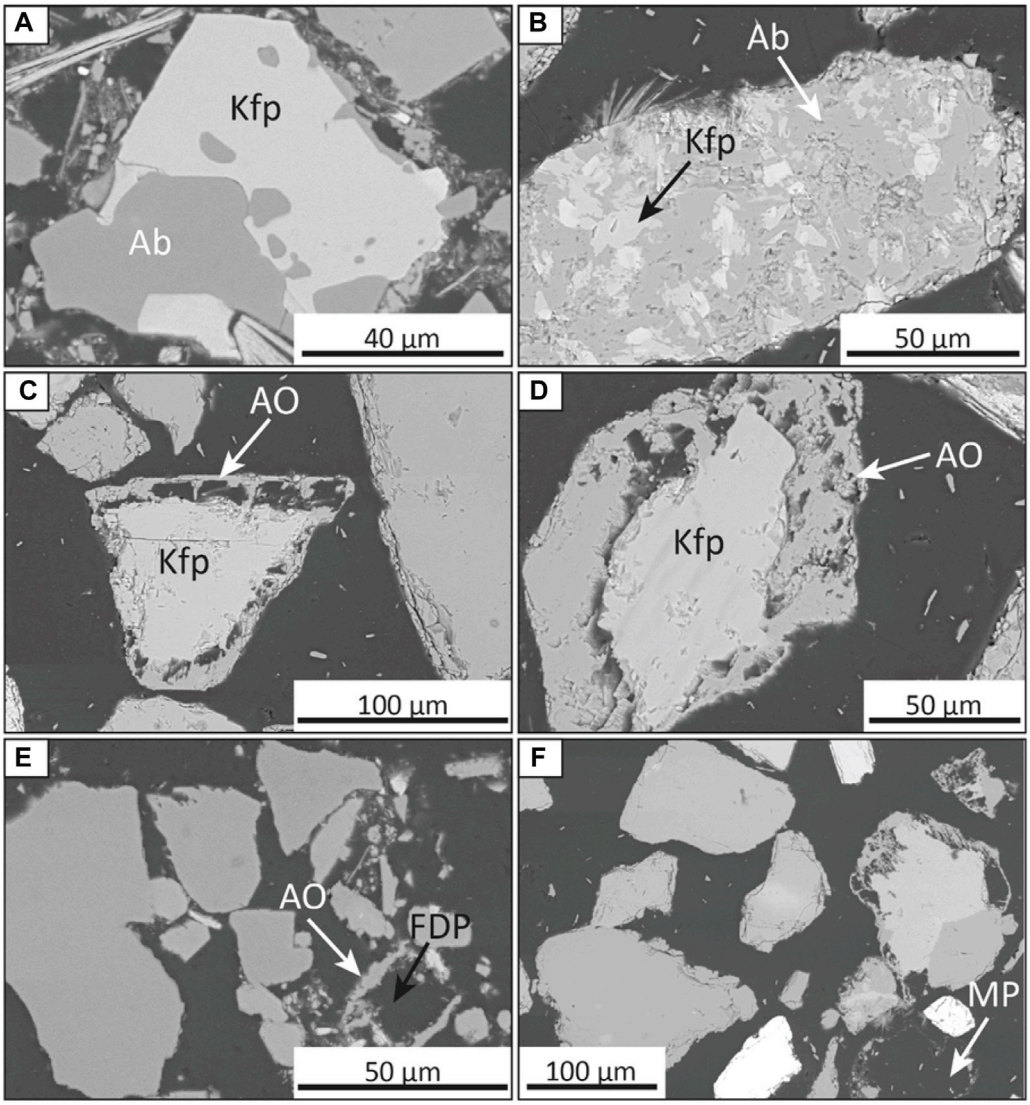

FIGURE 11
BSE images showing examples of albitization of feldspar, development of albite overgrowths, and dissolution of feldspars in the reacted samples of the Bute Inlet. **(A)** BSE image showing blocky albitization of K-feldspar (Kfp) (Sample 3). **(B)** BSE image showing pervasive albitization (Ab) of K-feldspar (Kfp) (Sample 3). **(C)** BSE image showing development of thin albite overgrowth (AO) (Sample 3). Note how the overgrowth grows into the dissolved K-feldspar, suggesting that the dissolution predated the development of the overgrowth. **(D)** BSE image showing the development of thick albite overgrowth (AO) on detrital K-feldspar (Sample 3). **(E)** BSE image showing dissolved feldspar grain being rimmed by albite overgrowth (AO), creating feldspar-dissolution porosity (FDP) (Sample 6). **(F)** BSE image showing a moldic pore (MP), formed from the complete dissolution of a feldspar grain (Sample 2). (BSE, Backscattered Electron).

In general, grain-coating chlorite can significantly inhibit the formation of authigenic quartz and albite overgrowths in deeply buried reservoirs by preserving porosity, and mica (biotite) grains can serve as important precursors for chlorite coats, especially in closed system diagenesis where Fe is readily available (Worden et al., 2020; Bello et al., 2022). In submarine fans, owing to hydrodynamic processes, high amounts of mica grains tend to be deposited in the distal fan (Mansurbeg et al., 2008; Marchand et al., 2015), implying the likelihood of forming high amounts of authigenic chlorite should mica (biotite) alteration occur. However, porosity will be significantly lost due to compaction if the mica content is high due to their high susceptibility to ductile deformation. Coatings of microquartz have been observed to prevent quartz and albite cementation in the reacted modern sediments of the Bute Inlet; therefore, sands rich in microquartz coatings would preserve reservoir quality should deep burial occur.

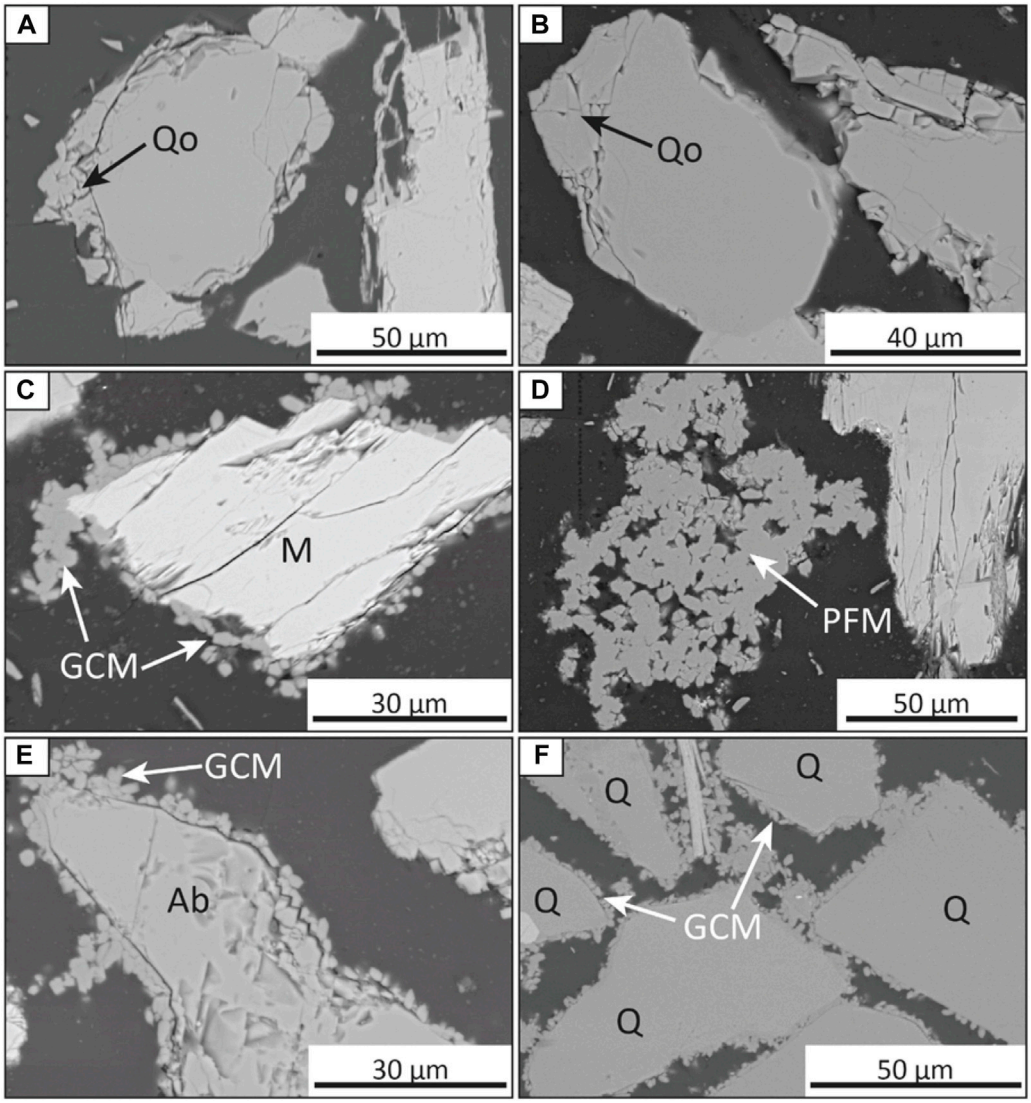

FIGURE 12
BSE images showing examples of quartz overgrowths, grain-coating, and pore-filling microcrystalline quartz in the reacted samples of the Bute Inlet. **(A)** BSE image showing blocky quartz overgrowth (Qo) (Sample 2). The pointed/sharp edges of the overgrowth suggest authigenic origin. **(B)** BSE image showing the formation of blocky quartz overgrowth (Qo) on detrital quartz (Sample 2). **(C)** BSE image showing grain-coating microquartz (GCM) coating detrital mica (Sample 2). **(D)** BSE image showing the development of pore-filling microcrystalline (PFM) quartz destroying intergranular porosity (Sample 2). **(E)** BSE image showing the formation of grain-coating microquartz (GCM) rimming detrital albite (Ab) (Sample 5). **(F)** BSE image showing the precipitation of microcrystalline quartz coating detrital quartz (Q), preventing the formation of macro quartz overgrowth (Sample 5). (BSE, Backscattered Electron).

Relation between hydrothermal reactor experiments and natural diagenesis

SEM-EDS observations have shown that chlorite coatings, which appeared to be recrystallized or neoformed, are similar in morphology to naturally-occurring chlorites. This suggests that the synthesized chlorite coatings are similar to those developed during natural diagenesis, in that both require precursors and a threshold temperature to form (Worden et al., 2020). Berthierine, for instance, is one of the common precursors for chlorite in sandstones, and transforms to chlorite at a threshold temperature between 90°C and 120°C (Aagaard et al., 2000; Worden and Morad, 2003; Chen et al., 2011; Charlaftis et al., 2021), whereas mica and inherited chlorite were the main precursors for chlorite in this study. Furthermore, although the sediment used in the hydrothermal reactor experiments for this study was heated to a temperature of 250°C to force the reaction to occur in a short time frame,

the temperature used is beyond the threshold required to form chlorite in natural diagenesis.

Even though the hydrothermal reactor experiments were carried out at conditions closely related to natural reservoirs, there are significant differences between the two: 1) the reactor experiments are characterized by short experimental time compared to natural diagenesis; and 2) the initial framework mineralogy of the starting material (mainly quartz and feldspar) as well as the artificial solution (Haile et al., 2015) are somewhat characterized by simple composition. In this study, for example, the experiments showed a path for chlorite development based on the initial mineralogy alone and predominantly from a single, chlorite precursor. This contrasts natural diagenesis where smectite, berthierine, kaolinite, and Fe-Mg rich lithic fragments (and siderite) can serve as precursors for chlorite (Iijima and Matsumoto, 1982; McKinley et al., 2003; Worden and Morad, 2003; Worden et al., 2020). Furthermore, unlike the experimental formation water, which has a specific composition at the start of the experiment, the formation water in natural sandstones might be either meteoric or marine during diagenesis, with a complex variation in composition and amount of dissolved cations.

Si and Al, among others, have been identified as essential ingredients for the formation of clay minerals (e.g., chlorite) in sandstone reservoirs (Worden and Morad, 2003; Haile et al., 2015; Worden et al., 2020). The Si and Al are sourced by reactive clays, redistribution of quartz, and alteration of plagioclase feldspar. In the reacted sediments of this study, the Si and Al incorporated into the authigenic chlorite formed might have been sourced from the reacted silica granules and dissolved plagioclase and K-feldspar grains. The study, therefore, demonstrates that, although Si and Al sourced from transformation of clay minerals are lacking, feldspar may serve as a potential source of Si and Al to form chlorite, while the alteration of detrital biotite and chlorite may have provided Fe and Mg as well as additional Si and Al. This is similar to what is in natural sandstones (Morad and Aldahan, 1987). Additionally, the decrease in albite content in the reacted Samples 5 and 6 and the corresponding high chlorite content (Table 2) support this interpretation.

Nevertheless, despite the similarities and differences between the hydrothermal reactor experiments and natural diagenesis, the study shows that the formation of chlorite on clean quartz and feldspar grains is possible and occurs quite fast (e.g., 72 h) at the studied experimental temperature of 250°C.

Implications for reservoir quality prediction in ancient turbidite reservoirs

Clean, clay-free sandstones are often thought to have the best reservoir quality; however, such sandstones are often susceptible to pervasive quartz cementation during burial. In contrast, sandstones with clay coatings could prevent quartz cementation at deep burial, thereby preserving reservoir quality (Heald and Larese, 1974; Pittman et al., 1992; Ehrenberg, 1993; Stricker and Jones, 2018; Tang et al., 2018; Busch et al., 2020). Our study has shown that the reacted sediments from the proximal channel, Station 028A (Samples 2 and 3; Table 2), have poorly developed chlorite coating coverage (max 47%) due to insufficient volume (<1%) of the main chlorite precursor. In addition, should they undergo deep burial (and chemical compaction), they would develop quartz and albite cements, which would significantly reduce reservoir quality. Nevertheless, the reacted sediments from the distal lobe Station 036 (Samples 5 and 6; Table 2) have better-developed chlorite coatings coverage (max 77%) due to higher volume (14.5%) of detrital chlorite precursors. Quartz and feldspar overgrowths are absent due to the well-developed chlorite coatings. However, while the proximal channel facies might be susceptible to extensive quartz cementation, should deep burial compaction occur, porosity in the distal fan facies might be significantly occluded by pore-filling chlorite, reducing reservoir quality.

Consequently, since the results of the experiments have shown that precursor detrital chlorite is essential for the continuous growth of diagenetic chlorite with increasing temperature, it is important to identify the depositional environments and processes in deep-water sandstones that could potentially lead to the formation and occurrence of diagenetic clay coats in ancient turbidite reservoirs (Bello et al., 2021). For instance, detrital clay coats in deep-water turbidites are reported to have been inherited from continental, transitional, and shallow marine/shelf environments before being transported to deep-water settings (Bahlis and de Ros, 2013; Yezerski and Shumaker, 2018; Bello et al., 2021). Thus, although such inherited coats might be susceptible to abrasion during transport, submarine channels, which are close to shelf, could potentially have remnant detrital clay coats that might recrystallize to form continuous, diagenetic coats during burial diagenesis, thereby preserving reservoir quality. In addition, detrital clay coats have been interpreted to form during sediment dewatering in submarine channels and lobe axis areas (Housenknecht and Ross, 1992; Collins et al., 2015; Porten et al., 2019; Bello et al., 2022), which could form diagenetic coatings at deeper burial. Even though the evidence of sediment-dewatering structures is absent in the studied cores of the proximal channel facies (e.g., Figure 2A), the presence of inherited, remnant chlorite coatings in the unreacted sediment from the proximal channel facies (Figure 2E) suggests that they have contributed to the formation of authigenic chlorite coatings in the reacted sediments. Furthermore, the occurrence of high mica content in low-energy, distal submarine fan owing to fractionation of turbidity currents based on grain shape and density (Mansurbeg et al., 2008; Stammer, 2014; Marchand et al., 2015), and their subsequent alteration, could lead to the formation of grain-coating chlorite to prevent quartz and albite cementation. Altered mica in the reacted distal lobe sediments (e.g., Figures 6F, 8E) have contributed to the formation of Fe-rich chlorite.

Conclusion

1) Hydrothermal reactor experiments simulating burial diagenesis conducted using modern-day proximal channel and distal lobe sediment samples, an artificial solution, and silica granules have resulted in the formation chlorite and microquartz coatings.
2) The experiments have identified the formation of chlorite and microquartz coatings on clean quartz and feldspar detrital grains, preventing the development of quartz and feldspar overgrowths.
3) Chlorite and detrital biotite have acted as precursors of authigenic chlorite coatings, morphologically similar to naturally-occurring chlorite coatings. Albite and K-feldspar dissolution have provided the required Al and Si for the formation of the chlorite coatings, whereas altered micas supplied the required Fe.
4) The experiments conducted using a silica supersaturated solution led to the formation of microquartz coatings, which prevented the development of quartz and feldspar overgrowths. Better developed chlorite coatings were formed during the experiments conducted without the silica supersaturated solution.
5) The formation of extensive chlorite coatings on detrital grains mainly depends on the volume of the initial precursor clay content. A distal lobe (Station 036) sample with an initial chlorite volume of 14.5% has increased to 42.9–56.3% post-experiment, generating 77% average chlorite-coating coverage on detrital grains. In contrast, a proximal channel (Station 028A) sample with less than 1% initial chlorite volume has developed an average chlorite-coating coverage of 47%.

Data availability statement

The raw data supporting the conclusion of this article will be made available by the authors, without undue reservation.

Author contributions

AB: Conceptualization, Data curation, Formal analysis, Funding acquisition, Core Sampling, Experiments, Methodology, Project administration, Software, Visualization, Writing–original draft, Writing–review and editing. DC: Experiments, Visualization, Writing–review and editing SJ: Conceptualization, Supervision, Resources, Validation, Visualization, Writing–review and editing. JG: Resources, Supervision, Validation, Writing–review and editing. SA: Supervision, Validation, Visualization, Writing–review and editing. MC: Supervision, Validation, Visualization, Writing–review and editing. KA-R: Visualization, Writing–review and editing. All authors contributed to the article and approved the submitted version.

Funding

Petroleum Technology Development Fund (PTDF), Nigeria. Award Number: PTDF/ED/PHD/BAM/1103/17.

Acknowledgments

The work contained in this paper was conducted during a PhD study funded by Nigerian Federal Government through Petroleum Technology Development Fund (PTDF), whose financial support is gratefully acknowledged. The authors are grateful to Ian Chaplin and Leon Bowen for preparation of thin sections and assistance in the use of SEM, respectively. We are equally grateful to Claire McGhee for her assistance in syringe-core sampling.

Conflict of interest

The authors declare that the research was conducted in the absence of any commercial or financial relationships that could be construed as a potential conflict of interest.

Publisher's note

References

Aagaard, P., Jahren, J. S., Harstad, A. O., Nilsen, O., and Ramm, M. (2000). Formation of grain-coating chlorite in sandstones. Laboratory synthesized vs . natural occurrences. *Clay Min.* 35, 261–269. doi:10.1180/000985500546639

Aase, N. E., Bjørkum, P. A., and Nadeau, P. H. (1996). The effect of grain-coating microquartz on preservation of reservoir porosity. *Am. Assoc. Pet. Geol. Bull.* 80, 1654–1673. doi:10.1306/64eda0f0-1724-11d7-8645000102c1865d

Aase, N. E., and Walderhaug, O. (2005). The effect of hydrocarbons on quartz cementation: Diagenesis in the upper jurassic sandstones of the miller field, North Sea, revisited. *Pet. Geosci.* 11, 215–223. doi:10.1144/1354-079304-648

Ahn, J. H., Peacor, D. R., and Coombs, D. S. (1988). Formation mechanisms of illite, chlorite and mixed-layer illite-chlorite in Triassic volcanogenic sediments from the Southland Syncline, New Zealand. *Contr. Mineral. Pet.* 99, 82–89. doi:10.1007/BF00399368

Ajdukiewicz, J. M., and Larese, R. E. (2012). How clay grain coats inhibit quartz cement and preserve porosity in deeply buried sandstones: Observations and experiments. *Am. Assoc. Pet. Geol. Bull.* 96, 2091–2119. doi:10.1306/02211211075

Al-Ramadan, K. (2014). Illitization of smectite in sandstones: The permian unayzah reservoir, Saudi arabia. *Arab. J. Sci. Eng.* 39, 407–412. doi:10.1007/s13369-013-0913-6

Al-Ramadan, K., Morad, S., Norton, A. K., and Hulver, M. (2013a). "Linking diagenesis and porosity preservation versus destruction to sequence stratigraphy of gas condensate reservoir sandstones; the Jauf Formation (Lower to Middle Devonian), Eastern Saudi Arabia," in *Linking Diagenesis to Sequence Stratigraphy*. Editor T. Stevens (Chichester, West Sussex, United Kingdom: Wiley-Blackwell), 297–336.

Al-Ramadan, K., Morad, S., and Plink-Björklund, P. (2013b). "Distribution of diagenetic alterations in relationship to depositional facies and sequence stratigraphy of a wave- and tide-dominated siliciclastic shoreline complex: Upper cretaceous chimney rock sandstones, Wyoming and Utah, USA," in *Linking diagenesis to sequence Stratigraphy*. (West Sussex, UK: John Wiley & Sons), 271–296. doi:10.1002/9781118485347.ch12

Al-Ramadan, K. (2021). The role of diagenesis at unconformities of the paleozoic siliciclastic succession of central Saudi Arabia: Implications for reservoir quality. *Arab. J. Geosci.* 14, 484. doi:10.1007/s12517-021-06845-6

Bahlis, A. B., and de Ros, L. F. (2013). Origin and impact of authigenic chlorite in the Upper Cretaceous sandstone reservoirs of the Santos Basin, eastern Brazil. *Pet. Geosci.* 19, 185–199. doi:10.1144/petgeo2011-007

Bello, A. M., Jones, S., Gluyas, J., Acikalin, S., and Cartigny, M. (2021). Role played by clay content in controlling reservoir quality of submarine fan system, Forties Sandstone Member, Central Graben, North Sea. *Mar. Petroleum Geol.* 128, 105058. doi:10.1016/j.marpetgeo.2021.105058

Bello, A. M., Jones, S. J., Gluyas, J., and Al-Ramadan, K. (2022). Impact of grain-coating clays on porosity preservation in paleocene turbidite channel sandstones: Nelson oil field, UK Central North sea. *Minerals* 12, 555. doi:10.3390/min12050555

Bloch, S., Lander, R. H., and Bonnell, L. (2002). Anomalously high porosity and permeability in deeply buried sandstone reservoirs: Origin and predictability. *Am. Assoc. Pet. Geol. Bull.* 86, 301–328. doi:10.1306/61eedabc-173e-11d7-8645000102c1865d

Boles, J. R. (1982). Active albitization of plagioclase, Gulf coast tertiary. *Am. J. Sci.* 282, 165–180. doi:10.2475/ajs.282.2.165

Bouma, A. H. (1962). *Sedimentology of some flysch deposits*, 168. Amsterdam: Elsevier, 168.

Busch, B., Hilgers, C., and Adelmann, D. (2020). Reservoir quality controls on Rotliegend fluvio-aeolian wells in Germany and The Netherlands, Southern Permian Basin – impact of grain coatings and cements. *Mar. Petroleum Geol.* 112, 104075. doi:10.1016/j.marpetgeo.2019.104075

Charlaftis, D., Dobson, K. J., Jones, S. J., Lakshtanov, D., Crouch, J., and Cook, J. (2022). Experimental simulation of burial diagenesis and subsequent 2D-3D characterization of sandstone reservoir quality. *Front. Earth Sci.* 10, 766145. doi:10.3389/feart.2022.766145

Charlaftis, D., Jones, S. J., Dobson, K. J., Crouch, J., and Acikalin, S. (2021). Experimental study of chlorite authigenesis and influence on porosity maintenance in sandstones. *J. Sediment. Res.* 91, 197–212. doi:10.2110/JSR.2020.122

Chen, G., Du, G., Zhang, G., Wang, Q., Lv, C., and Chen, J. (2011). Chlorite cement and its effect on the reservoir quality of sandstones from the Panyu low-uplift, Pearl River Mouth Basin. *Pet. Sci.* 8, 143–150. doi:10.1007/s12182-011-0127-z

Chowdhury, A. H., and Noble, J. P. A. (1993). Feldspar albitization and feldspar cementation in the Albert Formation reservoir sandstones, New Brunswick, Canada. *Mar. Petroleum Geol.* 10, 394–402.

Collins, J., Kenyon-Roberts, S., Cullen, B., White, J., Bordas-Le Floch, N., and Downey, J. (2015). Arran field: A complex heterolithic reservoir on the margins of the Forties fan system. *Geol. Soc. Spec. Publ.* 403, 185–217. doi:10.1144/SP403.10

Dutton, S. P., Hutton, M. E., Ambrose, W. A., Childers, A. T., and Loucks, R. G. (2018). Preservation of reservoir quality by chlorite coats in deep Tuscaloosa Sandstones, Central Louisiana, USA. *Gulf Coast Assoc. Geol. Soc.* 7, 46–58.

Ehrenberg, S. N. (1993). Preservation of anomalously high porosity in deeply buried sandstones by grain-coating chlorite: Examples from the Norwegian continental shelf. *AAPG Bull.* 77, 1260–1286.

French, M. W., Worden, R. H., King, H. E., Horn, W. C., Lamberti, W. A., and Shosa, J. D. (2021). The origin of silica cements revealed by spatially resolved oxygen isotope microanalysis and electron-beam microscopy; Heidelberg Formation, Germany. *Geochimica Cosmochimica Acta* 309, 57–78. doi:10.1016/j.gca.2021.06.019

French, M. W., Worden, R. H., Mariani, E., Larese, R. E., Mueller, R. R., and Kliewer, C. E. (2012). Microcrystalline quartz generation and the preservation of porosity in sandstones: Evidence from the upper cretaceous of the subhercynian basin, Germany. *J. Sediment. Res.* 82, 422–434. doi:10.2110/jsr.2012.39

French, M. W., and Worden, R. H. (2013). Orientation of microcrystalline quartz in the Fontainebleau Formation, Paris Basin and why it preserves porosity. *Sediment. Geol.* 284–285, 149–158. doi:10.1016/j.sedgeo.2012.12.004

Gales, J. A., Talling, P. J., Cartigny, M. J. B., Hughes Clarke, J., Lintern, G., Stacey, C., et al. (2018). What controls submarine channel development and the morphology of deltas entering deep-water fjords? *Earth Surf. Process. Landf.* 44, 535–551. doi:10.1002/esp.4515

González-Acebrón, L., Arribas, J., and Mas, R. (2010). Role of sandstone provenance in the diagenetic albitization of feldspars. *Sediment. Geol.* 229, 53–63. doi:10.1016/j.sedgeo.2010.06.005

Grigsby, J. D. (2001). Origin and growth mechanism of authigenic chlorite in sandstones of the lower vicksburg formation, south Texas. *J. Sediment. Res.* 71, 27–36. doi:10.1306/060100710027

Hage, S. (2019). *Turbidity current processes and products in the fjords of British Columbia (Canada)* (Canada: University of Southampton), 144. Doctoral Thesis.

Haile, B. G., Hellevang, H., Aagaard, P., and Jahren, J. (2015). Experimental nucleation and growth of smectite and chlorite coatings on clean feldspar and quartz grain surfaces. *Mar. Petroleum Geol.* 68, 664–674. doi:10.1016/j.marpetgeo.2015.02.006

Heald, M. T., and Larese, R. E. (1974). Influence of coatings on quartz cementation. *SEPM J. Sediment. Res.* 44, 1269–1274. doi:10.1306/212f6c94-2b24-11d7-8648000102c1865d

Heijnen, M. S., Clare, M. A., Cartigny, M. J. B., Talling, P. J., Hage, S., Lintern, D. G., et al. (2020). Rapidly-migrating and internally-generated knickpoints can control submarine channel evolution. *Nat. Commun.* 11, 3129. doi:10.1038/s41467-020-16861-x

Hendry, J. P., and Trewin, N. H. (1995). Authigenic quartz microfabrics in cretaceous turbidites: Evidence for silica transformation processes in sandstones. *J. Sediment. Res. A Sediment. Petrology Process.* 65, 380–392. doi:10.1306/d42680cc-2b26-11d7-8648000102c1865d

Hillier, S., and Velde, B. (1992). Chlorite interstratified with a 7 Å mineral: An example from offshore Norway and possible implications for the interpretation of the composition of diagenetic chlorites. *Clay Min.* 27, 475–486. doi:10.1180/claymin.1992.027.4.07

Houseknecht, D. (1987). Assessing the relative importance of compaction pro ces ses and cementation to reduction of porosity in sandstones. *AAPG Bull.* 6, 633–642.

Houseknecht, D. W., and Pittman, E. D. (1992). *Origin, diagenesis, and petrophysics of clay minerals in sandstones* (Oklahoma, United States: SEPM (Society for Sedimentary Geology). doi:10.2110/pec.92.47

Housenknecht, D. W., and Ross, L. M. (1992). *Clay minerals in Atokan deep-water sandstone facies, Arkoma Basin: Origins and influence on diagenesis and reservoir quality*, 47. Oklahoma, United States: Origin, diagenesis and petrophysics of clay minerals in sandstonesSEPM Special Publication, 227–278.

Hughes Clarke, J. E. (2016). First wide-angle view of channelized turbidity currents links migrating cyclic steps to flow characteristics. *Nat. Commun.* 7, 11896. doi:10.1038/ncomms11896

Iijima, A., and Matsumoto, R. (1982). Berthierine and chamosite in coal measures of Japan. *Clays Clay Min.* 30, 264–274. doi:10.1346/CCMN.1982.0300403

Jahren, J., and Ramm, M. (2000). "The porosity-preserving effects of microcrystalline quartz coatings in arenitic sandstones: Examples from the Norwegian continental shelf," in *Quartz cementation in sandstones*. (Oxford, UK: Blackwell Publishing Ltd.), 271–280. doi:10.1002/9781444304237.ch18

Khanam, S., Quasim, M. A., and Ahmad, A. H. M. (2021). Diagenetic control on the distribution of porosity within the depositional facies of proterozoic rajgarh formation, alwar sub-basin, northeastern Rajasthan. *J. Geol. Soc. India* 97, 697–710. doi:10.1007/s12594-021-1752-9

Lander, R. H., and Walderhaug, O. (1999). Predicting porosity through simulating sandstone compaction and quartz cementation. *Am. Assoc. Pet. Geol. Bull.* 83, 433–449. doi:10.1306/00aa9bc4-1730-11d7-8645000102c1865d

Lima, R. D., and De Ros, L. F. (2002). The role of depositional setting and diagenesis on the reservoir quality of Devonian sandstones from the Solimões Basin, Brazilian Amazonia. *Mar. Petroleum Geol.* 19, 1047–1071. doi:10.1016/S0264-8172(03)00002-3

Mansurbeg, H., Morad, S., Salem, A., Marfil, R., El-ghali, M. A. K., Nystuen, J. P., et al. (2008). Diagenesis and reservoir quality evolution of palaeocene deep-water, marine sandstones, the Shetland-Faroes Basin, British continental shelf. *Mar. Petroleum Geol.* 25, 514–543. doi:10.1016/j.marpetgeo.2007.07.012

Marchand, A. M. E., Apps, G., Li, W., and Rotzien, J. R. (2015). Depositional processes and impact on reservoir quality in deepwater Paleogene reservoirs, US Gulf of Mexico. *Am. Assoc. Pet. Geol. Bull.* 99, 1635–1648. doi:10.1306/04091514189

Matlack, K. S., Houseknecht, D. W., and Applin, K. R. (1989). Emplacement of clay into sand by infiltration. *J. Sediment. Petrology* 59, 77–87. doi:10.1306/212F8F21-2B24-11D7-8648000102C1865D

McBride, E. F. (1989). Quartz cement in sandstones: A review. *Earth. Sci. Rev.* 26, 69–112. doi:10.1016/0012-8252(89)90019-6

McKinley, J. M., Worden, R. H., and Ruffell, A. H. (2003). "Smectite in sandstones: A review of the controls on occurrence and behaviour during diagenesis," in *Clay mineral cements in sandstones*. 109–128. doi:10.1002/9781444304336.ch5

Milliken, K. L., McBride, E. F., and Land, L. S. (1989). Numerical assessment of dissolution versus replacement in the subsurface destruction of detrital feldspars, Oligocene Frio Formation, South Texas. *J. Sediment. Petrology* 59, 740–757. doi:10.1306/212F9061-2B24-11D7-8648000102C1865D

Morad, S., and Aldahan, A. A. (1987). Diagenetic chloritization of feldspars in sandstones. *Sediment. Geol.* 51, 155–164. doi:10.1016/0037-0738(87)90046-7

Morad, S., Bergan, M., Knarud, R., and Nystuen, J. P. (1990). Albitization of detrital plagioclase in triassic reservoir sandstones from the snorre field, Norwegian North Sea. *J. Sediment. Petrology* 60, 411–425. doi:10.1306/212F91AB-2B24-11D7-8648000102C1865D

Morad, S., Ketzer, J. M., and De Ros, L. R. (2000). Spatial and temporal distribution of diagenetic alterations in siliciclastic rocks: Implications for mass transfer in sedimentary basins. *Sedimentology* 47, 95–120. doi:10.1046/j.1365-3091.2000.00007.x

Pittman, E. D., Larese, R. E., and Heald, M. T. (1992). "Clay coats: Occurrence and relevance to preservation of porosity in sandstones," in *Origin, diagenesis, and petrophysics of clay minerals in sandstones*. (Oklahoma, United States: SEPM, Special Publication), 241–255. doi:10.2110/pec.92.47.0241

Porten, K. W., Warchol, M. J., and Kane, I. A. (2019). Formation of detrital clay grain coats by dewatering of deep-water sands and significance for reservoir quality. *J. Sediment. Res.* 89, 1231–1249. doi:10.2110/jsr.2019.65

Prior, D. B., and Bornhold, B. D. (1989). Submarine sedimentation on a developing Holocene fan delta. *Sedimentology* 36, 1053–1076. doi:10.1111/j.1365-3091.1989.tb01542.x

Prior, D. B., Bornhold, B. D., Wiseman, W. J., and Lowe, D. R. (1987). Turbidity current activity in a British Columbia fjord. *Science* 237, 1330–1333. doi:10.1126/science.237.4820.1330

Quasim, M. A., Khan, S., Srivastava, V. K., Ghaznavi, A. A., and Ahmad, A. H. M. (2021). Role of cementation and compaction in controlling the reservoir quality of the middle to late jurassic sandstones, jara dome, kachchh basin, Western India. *Geol. J.* 56, 976–994. doi:10.1002/gj.3989

Saigal, G. C., Morad, S., Bjorlykke, K., Egeberg, P. K., and Aagaard, P. (1988). Diagenetic albitization of detrital K-feldspar in Jurassic, Lower Cretaceous, and Tertiary clastic reservoir rocks from offshore Norway, I. Textures and origin. *J. Sediment. Petrology* 58, 1003–1013. doi:10.1306/212F8EE5-2B24-11D7-8648000102C1865D

Saner, S., Hassan, H. M., Al-Ramadan, K. A., and Abdulghani, W. M. (2006). Mineralogical, pore and petrophysical characteristics of the devonian jauf sandstone reservoir, hawiyah field, eastern Saudi arabia. *J. Pet. Geol.* 29, 257–272. doi:10.1111/j.1747-5457.2006.00257.x

Shaw, H. F., and Conybeare, D. M. (2003). "Patterns of clay mineral diagenesis in interbedded mudrocks and sandstones: An example from the palaeocene of the North Sea," in *Clay mineral cements in sandstones*. (International Association of Sedimentologists), 129–145. doi:10.1002/9781444304336.ch6

Stammer, J. G. (2014). *Hydrodynamic fractionation of minerals and textures in submarine fans: Quantitative analysis from outcrop, experimental, and subsurface studies*. (Colorado School of Mines). ProQuest Dissertations and Theses. Available at: http://search.proquest.com/docview/1610795911?accountid=8319%0A. http://fv8tn2mc8g.search.serialssolutions.com/?ctx_ver=Z39.88-2004&ctx_enc=info:ofi/enc:UTF-8&rfr_id=info:sid/ProQuest+Dissertations+%26+Theses+Global&rft_val_fmt=info:ofi/fmt:kev:mtx:disserta.

Stricker, S., and Jones, S. J. (2018). Enhanced porosity preservation by pore fluid overpressure and chlorite grain coatings in the Triassic Skagerrak, Central Graben, North Sea, UK. *Geol. Soc. Spec. Publ.* 435, 321–341. doi:10.1144/SP435.4

Tang, L., Gluyas, J., and Jones, S. (2018). Porosity preservation due to grain coating illite/smectite: Evidence from buchan formation (upper devonian) of the ardmore field, UK North Sea. *Proc. Geologists'. Assoc.* 129, 202–214. doi:10.1016/j.pgeola.2018.03.001

Taylor, T. R., Giles, M. R., Hathon, L. A., Diggs, T. N., Braunsdorf, N. R., Birbiglia, G. V., et al. (2010). Sandstone diagenesis and reservoir quality prediction: Models, myths, and reality. *Am. Assoc. Pet. Geol. Bull.* 94, 1093–1132. doi:10.1306/04211009123

Vagle, G. B., Hurst, A., and Dypvik, H. (1994). Origin of quartz cements in some sandstones from the jurassic of the inner moray firth (UK). *Sedimentology* 41, 363–377. doi:10.1111/j.1365-3091.1994.tb01411.x

Weibel, R., Friis, H., Kazerouni, A. M., Svendsen, J. B., Stokkendal, J., and Poulsen, M. L. K. (2010). Development of early diagenetic silica and quartz morphologies — examples from the siri canyon, Danish North Sea. *Sediment. Geol.* 228, 151–170. doi:10.1016/j.sedgeo.2010.04.008

Wilson, M. D. (1992). Inherited grain-rimming clays in sandstones from eolian and shelf environments: Their origin and control on reservoir properties. *Orig. Diagenesis, Petrophysics Clay Minerals Sandst.*, 209–225. doi:10.2110/pec.92.47.0209

Wooldridge, L. J., Worden, R. H., Griffiths, J., and Utley, J. E. P. (2019). How to quantify clay-coat grain coverage in modern and ancient sediments. *J. Sediment. Res.* 89, 135–146. doi:10.2110/jsr.2019.6

Worden, R. H., Griffiths, J., Wooldridge, L. J., Utley, J. E. P., Lawan, A. Y., Muhammed, D. D., et al. (2020). Chlorite in sandstones. *Earth-Science Rev.* 204, 103105. doi:10.1016/j.earscirev.2020.103105

Worden, R. H., Mayall, M., and Evans, I. J. (2000). The effect of Ductile-Lithic sand grains and quartz cement on porosity and permeability in Oligocene and lower Miocene clastics, South China Sea: Prediction of reservoir quality. *Am. Assoc. Pet. Geol. Bull.* 84, 345–359. doi:10.1306/c9ebcde7-1735-11d7-8645000102c1865d

Worden, R. H., and Morad, S. (2003). "Clay minerals in sandstones: Controls on formation, distribution and evolution," in *Clay mineral cements in sandstones* (Oxford, UK: Blackwell Publishing Ltd.), 1–41. doi:10.1002/9781444304336.ch1

Worden, R. H., and Morad, S. (2000). "Quartz cementation in oil field sandstones: A review of the key controversies," in *Quartz cementation in sandstones*. (Oxford: Wiley-Blackwell), 1–20. doi:10.1002/9781444304237.ch1

Yezerski, D. J., and Shumaker, N. (2018). "Improving prediction of porosity preservation in thermally-stressed deep marine sandstones: A synthesis of grain-coating chlorite," in *AAPG 2017 annual convention and exhibition* (Houston, Texas. Search and Discovery Article).

Zeng, J., Lowe, D. R., Prior, D. B., Wiseman, W. J., and Bornhold, B. D. (1991). Flow properties of turbidity currents in Bute inlet, British Columbia. *Sedimentology* 38, 975–996. doi:10.1111/j.1365-3091.1991.tb00367.x